Journal Pre-proof

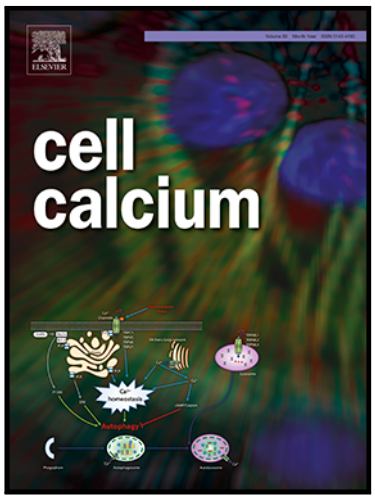

The physiological roles of anoctamin2/TMEM16B and anoctamin1/TMEM16A in chemical senses

Michele Dibattista , Simone Pifferi , Andres Hernandez-Clavijo , Anna Menini

PII: S0143-4160(24)00047-2
DOI: https://doi.org/10.1016/j.ceca.2024.102889
Reference: YCECA 102889

To appear in: *Cell Calcium*

Received date: 29 February 2024
Revised date: 11 April 2024
Accepted date: 17 April 2024

Please cite this article as: Michele Dibattista , Simone Pifferi , Andres Hernandez-Clavijo , Anna Menini , The physiological roles of anoctamin2/TMEM16B and anoctamin1/TMEM16A in chemical senses, *Cell Calcium* (2024), doi: https://doi.org/10.1016/j.ceca.2024.102889

The physiological roles of anoctamin2/TMEM16B and anoctamin1/TMEM16A in chemical senses

Michele Dibattista[1], Simone Pifferi,[2,*], Andres Hernandez-Clavijo[3] and Anna Menini[4*]

[1] Department of Translational Biomedicine and Neuroscience, University of Bari A. Moro, 70121 Bari, Italy.
[2] Department of Experimental and Clinical Medicine, Università Politecnica delle Marche, 60126 Ancona, Italy.
[3] Department of Chemosensation, Institute for Biology II, RWTH Aachen University, 52074 Aachen, Germany.
[4] Neurobiology Group, SISSA, Scuola Internazionale Superiore di Studi Avanzati, 34136 Trieste, Italy.

[*]corresponding author

Abbreviations
EOG electro-olfactogram, MeS methanesulfonate, NFA niflumic acid, OE olfactory epithelium, OR odorant receptor, OSN olfactory sensory neuron, VNO vomeronasal organ, VSN vomeronasal sensory neurons.

Highlights

- TMEM16B, also known as anoctamin2 (ANO2) and TMEM16A, or anoctamin1 (ANO1), encode for Ca^{2+}-activated Cl^- channels.
- In olfactory sensory neurons, TMEM16B contributes to amplify the odorant response, to modulate action potential firing, response kinetics and adaptation.
- In vomeronasal sensory neurons, TMEM16A and TMEM16B shape the pattern of action potentials increasing the interspike interval.
- In type I taste bud cells, TMEM16A is activated during paracrine signaling mediated by ATP.

Graphic abstract

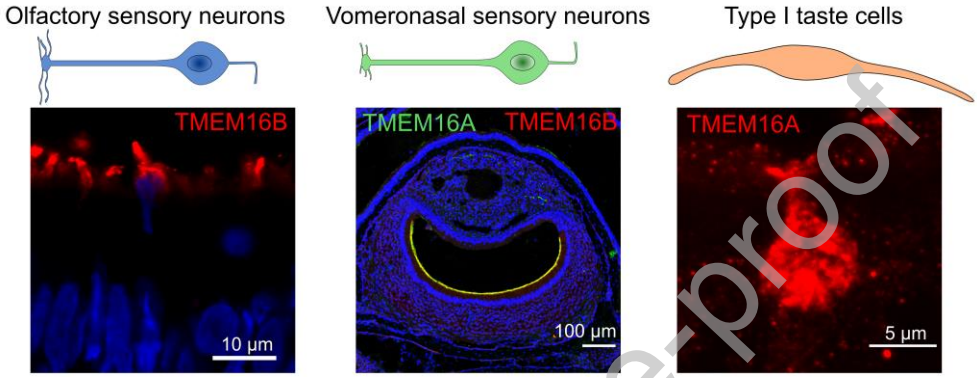

Abstract

Chemical senses allow animals to detect and discriminate a vast array of molecules. The olfactory system is responsible of the detection of small volatile molecules, while water dissolved molecules are detected by taste buds in the oral cavity. Moreover, many animals respond to signaling molecules such as pheromones and other semiochemicals through the vomeronasal organ. The peripheral organs dedicated to chemical detection convert chemical signals into perceivable information through the employment of diverse receptor types and the activation of multiple ion channels. Two ion channels, TMEM16B, also known as anoctamin2 (ANO2) and TMEM16A, or anoctamin1 (ANO1), encoding for Ca^{2+}-activated Cl^- channels, have been recently described playing critical roles in various cell types. This review aims to discuss the main properties of TMEM16A and TMEM16B-mediated currents and their physiological roles in chemical senses. In olfactory sensory neurons, TMEM16B contributes to amplify the odorant response, to modulate firing, response kinetics and adaptation. TMEM16A and TMEM16B shape the pattern of action potentials in vomeronasal sensory neurons increasing the interspike interval. In type I taste bud cells, TMEM16A is activated during paracrine signaling mediated by ATP. This review aims to shed light on the regulation of diverse signaling mechanisms and neuronal excitability mediated by Ca^{2+}-activated Cl^- channels, hinting at potential new roles for TMEM16A and TMEM16B in the chemical senses.

1. Introduction

TMEM16B, also known as anoctamin2 (ANO2) and TMEM16A, or anoctamin1 (ANO1) are two paralogous proteins within the TMEM16 protein family, which comprises eight additional members [1–4]. While TMEM16A and TMEM16B function as Ca^{2+}-activated Cl^- channels [5–9], most other TMEM16 proteins exhibit lipid scrambling activity (TMEM16C, D, E, F, K and J, [10–14], or fulfill diverse cellular functions (TMEM16C, G, and H [15–17]). Interestingly, some TMEM16 scramblases can also mediate ion channel activity (TMEM16D-F and J, [12,18–22]).

TMEM16B is predominantly expressed in neurons and plays a crucial role in regulating neuronal excitability [23]. In particular, TMEM16B is expressed in olfactory sensory neurons [8,24–32], vomeronasal sensory neurons [25,33–35], photoreceptors [26,36], lateral septum [37], cerebellar Purkinje cells [38], central lateral amygdala [39], nodose ganglion neurons [40], inferior olivary nucleus [41], dorsal root ganglion neurons [42], and hippocampal neurons [43]. Furthermore, TMEM16B is also expressed in the pineal gland [44] and retinal pigment epithelium [45].

In contrast, TMEM16A is mainly expressed in epithelia, where it regulates transepithelial Cl^- transport [23,46]. Additionally, TMEM16A plays a relevant role in controlling vascular tone by modulating the contraction of vascular smooth muscle cells [47,48]. Interestingly, TMEM16A is expressed in vomeronasal sensory neurons (VSNs) [26,28,33,33,34], controlling the firing pattern [34,35], and in glial-like type I taste bud cells, possibly regulating paracrine signaling within taste receptor cells [49,50].

This review will focus on the physiological roles of TMEM16B and TMEM16A in the olfactory epithelium, vomeronasal epithelium and taste buds. These peripheral structures of chemical senses are responsible for detecting specific molecules such as odorants, semiochemicals and tastants present in the external word.

2. Electrophysiological properties of TMEM16B and TMEM16A

Among the members of the TMEM16 family, TMEM16A and TMEM16B are the most similar, sharing about 60% amino acid identity [7], and they encode for Ca^{2+}-activated Cl^- channels. The electrophysiological properties of currents mediated by TMEM16B and TMEM16A are rather similar, although some differences may have a significant impact on the physiological processes controlled by these two proteins [51]. The three-dimensional structure of various TMEM16 family members, including TMEM16A, has been resolved, revealing a generally conserved organization. TMEM16 proteins are dimers, with each monomer composed of 10 transmembrane domains forming an independent pore [13,52–55]. Although the structure of TMEM16B remains undetermined, its high sequence similarity with other family members, alongside data from mutagenesis studies, suggests it shares this general structural organization [56,57].

TMEM16B primarily function as an anion channel, although it also has a small permeability to Na^+ (Fig.1A-C [8,9,57,58]). Under bi-ionic conditions, the relative anion selectivity sequence of TMEM16B is $SCN^->NO_3^->I^->B^->Cl^->F^-$, with larger anions such as methanesulfonate (MeS) and gluconate displaying a negligible permeability [8,9,57,58]. These permeability properties are nearly identical to those of TMEM16A [5–7,58,59]. Structural and mutagenesis experiments showed that the TMEM16A pore is amphiphilic and contains charged, polar, and apolar residues.

Cl^- binds to several positive charged amino acids such as K584, R617 and K641 [54,60–62]. Mutations of some of these homologous residues in TMEM16B cause alterations in ionic permeability and Ca^{2+} sensitivity, indicating a similar pore structure and permeability mechanisms [57]. Interestingly, chimera studies have shown that the pore region of TMEM16A increases the membrane expression of TMEM16B [58].

The activation of both these channels mainly depends on intracellular Ca^{2+} concentration. For TMEM16B, the dose response curve for Ca^{2+} activation has a voltage-dependent half-maximal effective concentration (EC_{50}) in the range 1.2-3.3 μM (at +40/+70 mV; Fig 1 D-E), a parameter influenced by factors such as clone species, splice variants and recording conditions (e.g., whole-cell vs. inside-out configuration, [8,9,57,58]. TMEM16A is slightly more sensitive to Ca^{2+} than TMEM16B, with an EC_{50} of 1-1.3 μM (at +60/+70mV) [54,58,63]. Structural and mutagenesis experiments on TMEM16A showed that the main Ca^{2+} binding domain contains several negatively charged residues in transmembrane domains 6 and 7, that can coordinate two Ca^{2+} ions [53,54,64]. These residues are conserved in TMEM16B, indicating a similar organization of the Ca^{2+} binding domain, although mutagenesis experiments to confirm this hypothesis are still needed. The localization of the Ca^{2+} binding domain within the membrane's electric field could explain the voltage-dependence Ca^{2+} sensitivity in both channels, although it has also been suggested that voltage-dependent conformational changes of the Ca^{2+}-binding site may play a role (Fig. 1E [53,54,65]).

TMEM16A and TMEM16B are modulated by membrane voltage despite lacking a canonical voltage-sensor domain [56,56,58,66]. In particular, TMEM16A can be activated even in the absence of Ca^{2+} at high membrane voltages, while it is unclear whether TMEM16B needs the presence of Ca^{2+} to be activated [66,67]. The voltage sensitivity of TMEM16A and TMEM16B-mediated currents strongly depends on intracellular Ca^{2+} concentration. Indeed, at low levels of Ca^{2+} the current shows a strong outward rectification and a clear time dependent relaxation, whereas at high levels of Ca^{2+} the current has a linear current-voltage relation without a time dependent component [66,68–70]. Moreover, it is well established that permeant ions allosterically modulate the voltage sensitivity of both channels. In particular, anions more permeant than Cl^-, such as SCN^-, shift the voltage dependence of the activation curve towards more negative values and increase the apparent Ca^{2+} sensitivity of TMEM16A and TMEM16B (Fig 1 F-G, [66,69,70]).

TMEM16A and TMEM16B can be blocked by several nonspecific blockers for Cl^- channels, including niflumic acid (NFA, [5,7–9]), 4'4'-Diisothiocyanatostilbene-2'2'-di-sulfonic acid (DIDS, [5,7,9]), 5-Nitro-2-(3-phenylpropylamino)benzoic acid (NPPB, [5,7,9]), and anthracene-9-carboxylic acid (A9C, [67,71,72]). Additionally, more specific blockers have been developed, such CaCCinh-01 [73], T16Ainh-A01 [74], MONNA [75], Ani9 [76], Benzbromarone [77]. It is important to highlight that among various blockers, Ani9 is the only one so far that it does not appear to disrupt intracellular Ca^{2+} signaling [78]. This distinction is crucial as the interference with Ca^{2+} signaling can complicate the interpretation of results when relying solely on a pharmacological approach. Specifically, Ani9 demonstrates selectivity for TMEM16A over TMEM16B when used at relatively low concentrations (1 μM, [76]).

TMEM16A and TMEM16B have different splicing variants [27,51]. For TMEM16B, four isoforms have been identified: A, $A_{\Delta4}$, B, $B_{\Delta4}$. The A variants have different starting codons, generating a protein with a longer intracellular N-terminus. The $A_{\Delta4}$ and $B_{\Delta4}$ isoforms lack exon 4, which encodes a stretch of four amino acid (EAVK) located in the first intracellular loop [8,27,36]. Interestingly, these two variants do not exhibit channel activity when expressed alone

heterologously, but they can modulate the properties of other variants containing exon 4 [27]. TMEM16B splicing variants have different expression patterns and slightly different electrophysiological properties, such as Ca^{2+} sensitivity and kinetics of Ca^{2+}-dependent inactivation [8,27,36].

3. TMEM16B and the sense of smell

3.*1 The olfactory epithelium*

Olfaction, the sense responsible for the perception of odorants, is activated by volatile molecules entering the nasal cavity through breathing, sniffing, or that are released from food during chewing [79,80]. Indeed, the olfactory epithelium (OE) is located within the olfactory cleft in the nose and some of these molecules bind to odorant receptors (ORs) present in the cilia of olfactory sensory neurons (OSNs, Fig. 2 A). OSNs are bipolar neurons that extend their dendritic branch to the apical region of the epithelium, terminating with a knob from which 10 to 20 cilia protrude. These cilia constitute an apical cellular compartment of about 0.1–0.2 μm in diameter and up to 100 μm in length, thus allowing OSNs to increase their surface-to-volume ratio, maximizing interactions with odorants [81,82]. The OE is a complex neuroepithelium composed also by other cell types some of which are now "gaining popularity" [83]. This increased attention is particularly evident in the case of supporting cells, which have taken "the center stage" during the recent COVID-19 pandemic [84]. Supporting cells are columnar-like cells with a apical membrane rich in microvilli and a basolateral membrane that closely interact with OSNs, almost enveloping them [81,82]. Furthermore, the OE contains a niche of basal stem cells, horizontal and globose cells, that ensure tissue regeneration and cellular turnover even in adulthood [85,86] (Fig 2 A).

3.2 Olfactory signal transduction

It is within the OSNs' cilia that the proteins involved in signal transduction are abundantly expressed. The chain of events leading to generation of a receptor current begins with the binding of an odorant molecule to an OR that in turn activates the stimulatory alpha subunit of a G protein: Gαolf. Activated Gαolf then increases the enzymatic activity of adenylyl cyclase type III (ACIII), thus increasing intraciliary cAMP concentration. Acting as a second messenger, cAMP binds to the CNG channel, increasing its open probability and allowing the influx of Na^+ and Ca^{2+} ions, thus generating an initial current. Several mechanisms including buffering by mitochondria maintain relatively low resting Ca^{2+} concentrations inside the cilia. The CNG channels are highly permeable to Ca^{2+} [87–89], whose concentration rapidly increases inside the OSN's cilia following odorant stimulation [90,91]. Spatially restricted odor pulses increased Ca^{2+} only in the stimulated cilia, further proving that each cilium of an OSN behave as a fully functional signaling compartment [91]. The surge in intracellular Ca^{2+} increases the open probability of a second set of channels: the Ca^{2+}-activated Cl^- channels (Fig. 2 B). The Ca^{2+}-activated Cl^- conductance was first described in 1991 [92] in OSNs from frogs and subsequently identified in the OSNs of various vertebrates, including fish, amphibians, and rodents [93–97]. However, identifying the molecular identity of the channel responsible for this current, now known to be TMEM16B, remained elusive for almost 25 years, as extensively reviewed by Pifferi et al. [98] and Dibattista et al. [31].

Remarkably, OSNs (and VSNs, see section 5 of this review) maintain an unusually high intraciliary Cl^- concentration, mainly through the activity of the Na^+-K^+-$2Cl^-$ cotransporter NKCC1 [99,100]. As the Cl^- concentrations in the nasal mucus, where the cilia are embedded, and

within the apical dendritic region of OSNs have a similar value of approximately 50 mM [101–103], the opening of TMEM16B will allow the efflux of Cl^-, contributing to OSNs depolarization. Employing Cl^- as the charge carrier in transduction gives the advantage of a reduced dependence on mucosal ion concentration, as cilia are immersed in the nasal mucus which is prone to composition fluctuations due to direct exposure to the external environment [104,105].

The termination of the odorant response involves several mechanisms that lead to the closure of both the CNG and TMEM16B channels. CNG channels gradually close with cAMP diffusion out of the ciliary space and/or its breakdown by phosphodiesterase, PDE1C and PDE4A [106]. Closure of TMEM16B channels mainly occurs through the removal of Ca^{2+} from the cilia, primarily through the action of the potassium-dependent Na^+/Ca^{2+} exchanger 4 (NCKX4) [107]. Furthermore, mitochondria located in the dendritic knob facilitate Ca^{2+} clearance following odorant exposure [108].

3.2.1 TMEM16B in olfactory transduction

Several studies clearly showed that TMEM16B encodes for the Ca^{2+}-activated Cl^- channels of OSNs[30,32,34,107,109] reviewed in [98] and [31]. All the spice variants of TMEM16B are expressed, but the isoforms B is the more abundant [27]. Recent evidence has also shown the expression of TMEM16B in human olfactory cilia, suggesting its involvement in olfactory signal transduction also in humans (Fig. 2C, ([110]). This hypothesis was initially supported by the anecdotal report of the widow of a patient affected by the type 3 von Willebrand (VWD) disease that involve 253 kb deletion in chromosome 12 producing the deletion of the VW factor gene and of the N-terminus of the neighboring Tmem16b gene. She declared that her late husband might have been unable to smell [8]. It was later shown that members of a large Italian family carrying the VWD because of the 253 kb deletion had no apparent olfactory deficits when tested using the University of Pennsylvania Smell Identification Test. As mentioned in section 2, splice variants for TMEM16B with a shortened N-terminus are the most abundantly expressed in OSNs leading leading to the hypothesis that they may be sufficient to ensure Ca^{2+}-activated Cl^- current in odorant signal transduction [8,111,112]. Further increasing the VWD patients sample size for the olfactory tests and coupling those with patients' biopsies would help to clarify this issue.

What is the role of the depolarizing Ca^{2+}-activated Cl^- currents via TMEM16B in olfactory transduction? Answering this question has been puzzling and perplexing. Nonetheless, the contribution of Ca^{2+}-activated Cl^- currents to signal transduction could be summarized in three points: 1. Amplification of the odorant response; 2. Modulation of firing; and 3. Response kinetics and adaptation.

3.2.1.1 Amplification of the odorant response

The odorant transduction cascade resembles an avalanche, progressively intensifying and expanding in scale (Fig. 2 B). Once initiated by odorant binding to the OR, there is a gradual amplification of the earlier steps, leading to cooperative effects. This amplification strictly depends on Ca^{2+}-activated Cl^- currents, indeed the Hill coefficient of cAMP-mediated current is approximately 1.5, while for the odorant response curve of intact OSNs, ranges from 3.5 to 5.4 [94,97,113]. This substantial increase underscores the role of the secondary Ca^{2+}-activated Cl^- currents in enhancing the nonlinear amplification of the receptor current [94,113]. It is worth noting that the small single channel conductance and the high open probability of Ca^{2+}-activated Cl^- currents optimize the signal-to-noise ratio, offering several advantages to odorant responses [114].

The amplifying role of Ca2+-activated Cl^- currents was confirmed by the generation of *Tmem16b* KO mice [25,30,115]. Indeed, the Ca^{2+}-activated Cl^- current was absent in OSNs of the *Tmem16b* KO mice (Fig. 3 A,B [30,34,115]). Moreover, the blocker NFA failed to further reduce the remaining ciliary current in OSNs from KO mice, confirming that TMEM16B is responsible for Ca^{2+}-activated Cl^- channels in OSN cilia (Fig. 3 A,B). In addition, the Cl^- contribution is substantial at various odorant concentrations and the amplification factor is highest at the signaling threshold, decreasing at saturation of the total response [115].

3.2.1.2 Modulation of OSN firing

The receptor current induced by odorants causes the generator potential, which may lead to firing in OSNs. Suction electrode recordings have consistently shown that OSNs usually fire 2-3 action potentials in response to stimulation [116–119]. At elevated odorant concentrations, the receptor current can be sustained for extended periods, as long as the stimulus is present, without eliciting additional action potentials (Fig. 3C). This phenomenon is caused by a reduction in the length of the action potential train, a result of the progressive decreasing amplitude of subsequent action potentials (Fig. 3C). This reduction is likely depending on inactivation of voltage-gated Na^+ and Ca^{2+} channels during prolonged depolarization [120,121].

The current flowing through the CNG channels is necessary and sufficient to elicit action potentials in OSNs due to their high input resistance [122,123]. While it may initially appear that the Ca^{2+}-activated Cl^- current is dispensable for odorant signal transduction [25], the importance of this current in modulating both the frequency of firing and the duration of the spike train in response to stimulation has been elucidated [30]. Indeed, OSNs from *Tmem16b* KO mice, exhibiting reduced transduction currents, surprisingly displayed a higher frequency of action potential compared to WT mice. Furthermore, the knockout of *Tmem16b* resulted in a significant prolongation of the action potential train (Fig. 3 D). These findings suggest that the depolarizing Ca^{2+}-activated Cl^- current acts as a "clamper", shortening firing by tuning it with the strength of odorant stimulus [30,115]. This modulation alters the time course of the response, leading to rapid inactivation of voltage-dependent Na^+ channels [120,121].

Removing the clamping effect of the Ca^{2+}-activated Cl^- current (Fig. 3D), could lead to an excessive firing frequency and prolonged spike trains, potentially interfering with the coding process in the next stage of the signal's journey: the olfactory bulb in the brain. Indeed, *Tmem16b* KO mice exhibit increased Ca^{2+} responses in the axon terminals of OSNs within the olfactory bulb [124], likely contributing to the altered naïve behavior observed in those mice [30,109]. Interestingly, in the Go/NoGo task, a training-dependent operant conditioning paradigm, the *Tmem16b* KO mice did not show any olfactory deficits [25]. This apparent conundrum could be explained by the ability to recognize odor with great accuracy within 200 ms [125–127] using an olfactometer. This brief time window could suffice for Tmem16b KO mice to identify a single monomolecular odorant during a solitary sniff, despite any alterations in odorant-induced action potentials. Conversely, in tasks where mice must locate a food source, which continually emits its odor plume within the cage, the olfactory system of *Tmem16b* KO mice might be overwhelmed (e.g., prolonged firing duration, modified adaptation), given the constant presence and diffusion of the odor.

3.2.1.3 Response kinetics and adaptation

To elucidate TMEM16B's role in shaping the kinetics of the overall odorant response, electro-olfactogram (EOG) recordings, an extracellular field technique that record the summated generator potentials of all responsive OSNs to odorants, is often used. Despite differing experimental conditions and odorants used, leading to some contrasting or paradoxical results [32,34,109], the importance of TMEM16B in modulating the overall shape of the odorant response has become apparent. Air-phase EOG recordings, in which the semi-intact OE is stimulated with odorants delivered through puffs of humidified air, have revealed that the absence of TMEM16B results in faster rise times and response termination [32]. These findings are particularly interesting as response termination plays a pivotal role in governing adaptation to repeated stimulations (Fig. 3 E, F).

Adaptation in OSNs in response to continuous or repetitive odorant stimulation is a critical mechanism preventing signal transduction overload [128]. This process is characterized by diminishing responses to repeated exposure to the same stimuli or sustained stimulation over time, ensuring sensitivity to new odorants while being exposed to constant or repetitive stimulation [129,130]. Such adaptation is mediated by Ca^{2+} influx through CNG channels, initiating various feedback loops. Among them, the CNG channel itself is influenced by a feedback mechanism where Ca^{2+} -calmodulin lowers the channel's cAMP affinity [129,131,132]. In addition to the CNG channel, ACIII has also been proposed as a potential feedback target for Ca^{2+} dependent adaptation via Ca^{2+}/CaMKII pathways, particularly for adaptation induced by sustained odor stimulations [133,134]. However, some evidence suggests that Ca^{2+}/CaMKII-mediated phosphorylation inhibiting ACIII may not play a substantial role in the adaptation process [135].

When two brief odorant pulses are delivered, the amplitude of the response to the second pulse is decreased [129,136] and the current amplitude gradually recovers to the initial value as the interval between odorant pulses increases (a stimulation protocol known as paired pulse protocol). Indeed, excessively long, or short response termination can alter the response to subsequent stimulation. The faster response termination observed in *Tmem16b* KO mice altered their adaptation profile, leading to earlier recovery of responses to shorter stimulation intervals compared to WT mice. Notably, TMEM16B, together with NCKX4 [107], acts synergistically to regulate response termination and adaptation. NCKX4 knockout OSNs display prolonged response termination by up to several seconds, as preventing Ca^{2+} extrusion leads to a prolonged Ca^{2+}-activated Cl^- current [137,138].

4. TMEM16 family members in supporting cells of the OE

Despite their name, supporting cells have a role that goes beyond merely supporting OSNs, as they may also participate in modulating the olfactory signal transduction pathway, indirectly influencing olfactory sensitivity and perception. Supporting cells are electrically coupled by gap junctions, composed at least by connexin 43 and 45, which form a syncytium for the diffusion of Ca^{2+} and other signaling molecules throughout the epithelium [139–141]. Supporting cells are involved in several physiological roles, including the metabolic processing of external substances and the production of various neurotrophic and neuromodulatory molecules such as endocannabinoids, insulin, and ATP, contributing to the regulation of neuronal function and overall neuronal health [142–149].

4.1 *TMEM16A in murine olfactory supporting cells*

TMEM16A is strongly expressed in the supporting cells of adult mice, mainly in the apical surface of the ventral region of the OE, particularly near the transition zone with the respiratory epithelium. TMEM16A is predominantly located in the apical part and in microvilli of supporting cells, with no detectable expression in OSNs [26,28,29,150].

Electrophysiological studies from both WT and *Tmem16a* KO mice have demonstrated that Ca^{2+}-activated Cl^- currents can be recorded in supporting cells and that TMEM16A is necessary to generate those currents [150]. The apical region and microvilli of supporting cells, like the cilia of OSNs, are immersed in nasal mucus, where the Cl^- concentration is approximately 50 mM. Interestingly, the cytosolic Cl^- concentration in supporting cells is about 30 mM [101] which would give a Cl^- equilibrium potential of *circa* -14 mV. Considering that supporting cell resting membrane potential has been reported to fall somewhere between -50 mV and -30 mV, the estimated electrochemical driving force for Cl^- suggests that the opening of TMEM16A could lead to a Cl^- efflux, potentially influencing the ionic composition within the nasal mucus covering the olfactory epithelium [150].

Moreover, TMEM16A in supporting cells may participate in the modulation of purinergic signaling. It has been reported that in the OE, there may be both constitutively and stimulated ATP release [149]. Activation of purinergic receptors by ATP triggers intracellular Ca^{2+} release, which is sufficient to activate TMEM16A-mediated Ca^{2+}-activated Cl^- currents in supporting cells [150]. ATP, acting via P2Y purinergic receptors expressed in supporting cells [151–153], may influence various processes such as neuroproliferation and neuroprotection within the OE, highlighting the multifaceted role of supporting cells in olfactory physiology.

4.2 TMEM16F in human olfactory supporting cells

It is important to notice that TMEM16A expression in supporting cells has been reported in mouse OE. However, unlike murine olfactory supporting cells, supporting cells of the human OE are known to express TMEM16F (Fig. 2D) [154]. Notably, during the COVID-19 pandemic, the loss of smell emerged as a distinctive symptom of infection, with supporting cells identified as the primary target of SARS-CoV-2 in the OE due to their expression of Angiotensin Converting Enzyme 2 (ACE2) on their cell membrane, unlike OSNs that do not express ACE2 [84,154–156]. Indeed, ACE2 is the cellular receptor for the SARS-CoV-2 spike protein, which facilitates virus-cell adhesion and the fusion process necessary for viral entry into the cell [157,158]. In some tissues, there is a formation of syncytia when the SARS-CoV-2 Spike protein, expressed on the surface of an infected cell, interacts with ACE2 receptors on neighboring cells. Subsequently, the scramblase TMEM16F is activated, leading to the exposure of phosphatidylserine to the external side of the membrane that acts as signaling for cell-to-cell fusion [159,160].Thus, following infection by SARS-CoV-2, supporting cells allow the virus to replicate, triggering an inflammatory response in the OE and/or the formation of syncytia that will disrupt OSNs function, consequently altering the sense of smell [84,154,161]. Supporting cells envelop OSNs dendrites, particularly as the neurons mature, creating a complex cell-in-cell arrangement. This structural intimacy implies that any disruption to supporting cells, such as syncytia formation, could directly impact the function of OSNs, thereby affecting olfactory function.

Furthermore, TMEM16F in the apical membrane of human supporting cells could also, similar to TMEM16A in murine supporting cells, function as an ion channel and alter the nasal mucus's ionic composition due to its permeability to a range of ions, including Cl^-, Ca^{2+}, and Na^+ [22].

5. TMEM16A and TMEM16B roles in pheromone detection within the vomeronasal organ

5.1 Sensory transduction in the VNO

The vomeronasal organ (VNO), a blind ended cylindrical structure located on the floor of the nasal cavity, plays a pivotal role in detecting socially relevant molecules, particularly pheromones and other semiochemicals, that regulate the physiology and behavior of several animals [162–165]. The VNO is composed of two epithelia, sensory and non-sensory epithelium, running parallel in the anterior-posterior axes and separated by a mucus-filled lumen. While the non-sensory epithelium primarily provides muscular contraction, essential for the pumping mechanism required for molecules to reach the lumen [166], the main function of the sensory epithelium is to capture such molecules, transducing the chemical signal into an electrical one, and relaying this information to the brain. This chemosensory transduction takes place within the vomeronasal sensory neurons (VSNs), the main cellular constituents of the sensory epithelium [164,165,167].

VSNs express specific vomeronasal receptor proteins in their microvillar membrane, facing the VNO luminal space. These are G protein-coupled receptors belonging to different family and are expressed in different subpopulations of VSNs [162,165,168–170]. The activation of specific G proteins initiates a PLC-mediated signal transduction cascade leading to the production of diacylglycerol (DAG) and inositol trisphosphate (IP3). DAG directly gates the cation channel TRPC2 allowing a depolarizing influx of Na^+ and Ca^{2+} (Fig. 4A) [171,172]. The increase of intracellular Ca^{2+} concentration activated different pathway both excitatory and inhibitory. Indeed, Ca^{2+} can activate non selective cationic channels [173,174], SK3 potassium channel [175], calmodulin controlling adaptation [174] and Cl^- channels [33,35,176–178].

5.1 TMEM16A and TMEM16B in vomeronasal transduction

Ca^{2+}-activated Cl^- currents in VSNs have been reported in several studies using different approaches [25,33–35,176–178]. In particular, Dibattista et al. [178] employed photorelease of caged Ca^{2+} to spatially and temporally control Ca^{2+} levels, demonstrating that Ca^{2+}-activated Cl^- channels are localized in the apical region and microvilli of VSNs (Fig 4 C,D; [178]).

Consistent with these functional data, immunolocalization showed that TMEM16A and TMEM16B are both expressed on the luminal surface of the vomeronasal sensory epithelium (Fig 5A, [26,34,178]). Immunocytochemistry performed on dissociated VSNs has further demonstrated that each VSN expresses both TMEM16A and TMEM16B, which co-localize on the microvilli of VSNs (Fig. 4B, [178]). This is particularly noteworthy, as VSNs are a rare example of cellular co-expression of both TMEM16A and TMEM16B. To our knowledge, only pinealocytes have been shown to co-express both TMEM16A and TMEM16B [44].

VSNs, like OSNs, maintain elevated internal Cl^- concentrations. In VSNs, this concentration varies from approximately 40 mM in the apical region [179] to about 85 mM in the soma [180]. Depending on the equilibrium potential of Cl^-, the concentration of which in the vomeronasal mucus is still unknown, the opening of Ca^{2+}-activated Cl^- channels in the microvilli of VSNs could induce a depolarizing Cl^- efflux that amplifies the primary cationic current, similar to what happens in olfactory transduction in OSNs, or may play a stabilizing role, preventing strong depolarizations.

A comprehensive electrophysiological characterization of the Ca^{2+}-activated Cl^- currents in VSNs showed that their properties more closely resemble those of heterologously expressed TMEM16A rather than TMEM16B channels [33]. While, when TMEM16A and TMEM16B were heterologously co-expressed, they formed a heteromeric channels that showed biophysical properties intermediate between those characteristic of each individual channel [44]. Moreover, the conditional knockout of *Tmem16a* in mature VSNs abolished Ca^{2+}-activated Cl^- currents, demonstrating that TMEM16A is an essential component of these currents in mouse VSNs [33–35]. In contrast, deletion of *Tmem16b* did not significantly altered Ca^{2+}-activated Cl^- currents in VSNs confirming the relevant role of TMEM16A (Fig. 5B, [34,35]). The role of TMEM16B in this context remains puzzling. We can speculate that the expression level of TMEMB in VSNs is relatively low, generating a negligible current (Ibarra-Soria *et al.*, 2014) or that the splice variants expressed in VSNs (such as isoform $A_{\Delta 4}$ and $B_{\Delta 4}$) are unable to form functional channels without TMEM16A [27]. Although TMEM16A and TMEM16B are co-expressed in VSNs, we still lack evidence confirming or refuting the formation of heteromeric channels in this system.

Even though TMEM16B expression seems not to be necessary to generate Ca^{2+}-activated Cl^- currents in VSNs, investigations on KO mice model shown that both TMEM16A and TMEM16B modulate the firing patterns in response to natural ligands [34,35]. Extracellular recordings measuring spiking activity demonstrated that the individual deletion of either *Tmem16a* or *Tmem16b* does not modify the spiking frequency of VSNs responses to pheromones (Fig. 5C-D; [35]). However, analysis of inter-spike-distribution revealed that both TMEM16A and TMEM16B contribute to shaping pheromone-evoked firing activity by prolonging inter-spike intervals (Fig. 5E-F). A study conducted in a *Tmem16a/Tmem16b* double KO mouse model [34] indicated that VSNs lost their ability to respond to natural ligands stimulation, although some innate VNO-dependent behavior remained unaltered. These conflicting findings underscore the need for a detailed study of the firing activity, response to natural stimuli and overall functionality of VSNs in mice lacking both TMEM16A and TMEM16B.

6. TMEM16A in taste buds

In mammals, the primary taste receptor cells are organized in taste buds, mainly localized in papillae on the tongue. Taste buds resemble onion-shaped structures composed of 50-100 tightly packed elongated epithelial cells (Fig. 6A). Based on their physiological role, taste bud cells can be categorized into three types. About half of taste bud cells are type I cells, which function as glial-like supportive cells [181,182]. Despite expressing the amiloride-sensitive Na^+ channel ENaC, it has been established that type I cells do not play a significant role in salt transduction [181,183–185]. Type II cells express different types of GPCRs for the transduction of sweet (TAS1R2, TAS1R3), umami (TAS1R1, TAS1R3) and bitter (TAS2Rs) tastants. These tastants activate a common pathway involving the G-protein α-subunit gustducin (GNAT3) and phospholipase-C β2, leading to an increase in intracellular Ca^{2+} concentration [186,187]. Ca^{2+} directly gates the cation channels TRPM5 and TRPM4, inducing cell depolarization, action potential firing, and release of ATP through the voltage-gated channel CALHM1/CALHM3 [188,189]. ATP subsequently activates the ionotropic receptor P2X2/3 in the afferent fiber to the central nervous system [190]. Type III cells mediate sour detection through the activation of the proton channel OTOP1, inducing intracellular acidification and blocking the inward rectifier K^+ channel KCNJ2, thus contributing to amplification of depolarization [191–193].

Several reports indicate that taste bud cells express Ca^{2+}-activated Cl^- channels [194–197,197,198]. By RT-PCR and immunohistochemistry Cherkashin et al. (2016) showed that both TMEM16A and TMEM16B are expressed in taste buds. However, more precise investigations using KO-verified antibodies and a mouse model expressing mCherry under *Tmem16b* promoter revealed that only TMEM16A is expressed in a subpopulation of taste bud cells (Fig. 6 B; [41,49]). Specifically, TMEM16A is mainly localized in the apical portion of type I cells, as demonstrated by the colocalization with the inward rectifier K^+ channel KCNJ1 (Fig. 6C, [49,199]). Electrophysiological recordings further confirmed that only type I cells show Ca^{2+}-activated Cl^- currents mediated by TMEM16A (Fig. 6D;[49]). Interestingly, stimulation of type I cells with ATP induced a TMEM16A-mediated current through the activation of metabotropic P2Y receptors (Fig. 6E; [49,198,200]).

The physiological roles of TMEM16A in taste bud cells are not yet fully understood, but various scenarios have been proposed. To understand the function of TMEM16A, knowledge of the equilibrium potential of Cl^- is crucial. Unfortunately, the intracellular Cl^- concentration is unknown and it is likely that the extracellular Cl^- concentrations vary between the basolateral and apical membrane. The latter is likely immersed in saliva containing about 44 mM of Cl^- [201,202], while the interstitial fluid facing the basolateral membrane contains about 100-110 mM of Cl^-. Moreover, the presence of salty tastants can dramatically alter the Cl^- concentration in the apical portion of the taste bud shifting the equilibrium potential of Cl^-.

Using intact taste bud preparations, Rodriguez et al. [50] reported that the activation of type II cells by bitter compounds induced an increase of intracellular Ca^{2+} concentration in type I cells, mediated by the activation of P2Y receptors through ATP released from type II cells. Therefore, TMEM16A could be physiologically activated by stimulation of type II cells (Fig. 6F). In the central nervous system, the activation of glia cells, such us astrocytes, during synaptic transmission is well studied and it can modulate neuronal activity at the circuit level [203,204]. In taste buds, different cell types could release various neurotransmitters, such as ATP, GABA and serotonin, mediating paracrine signaling possibly contributing to shape the firing of afferent fibers [182,205]. In this context, depolarization or hyperpolarization of type I cells mediated by TMEM16A could trigger the release of GABA or other neurotransmitter from type I cells [205,206]. Interestingly, type I cells express the Ecto-ATPase NTPDase2, which could contribute to regulate the ATP concentration surrounding the cells and therefore their response to ATP [50,207].

Buffering extracellular K^+ ions is a critical function performed by glial cells, mediated by various types of inward rectifier K^+ channels [208,209]. In type I cells, TMEM16A colocalizes with the KCNJ1 channel. Therefore, it can be envisioned that stimulation of type II cells, leading to the release of ATP, could produce an increase in intracellular Ca^{2+} in type I cells activating TMEM16A. Activation of TMEM16A would allow for the influx of Cl^- necessary to maintain the apical extrusion of K^+ through KCNJ1 channels [199].

7. Conclusions and Future Perspectives

Investigating peripheral sensory detection is important for understanding the mechanisms underlying the generation of electrical signals that are subsequently transmitted to higher centers in the brain, ultimately influencing behaviors. This task is particularly critical for chemical senses due to the complex nature of chemical stimuli.

Olfactory sensory neurons must be finely calibrated to possess an optimal range of sensitivity towards odorants, along with appropriate kinetics to effectively generate action

potentials. In this review, we discussed evidence indicating that a key determinant of these characteristics is TMEM16B, expressed in the cilia of olfactory sensory neurons. TMEM16B mediates a depolarizing Ca^{2+} activated Cl^- current during odorant response, crucial for regulating its amplitude and kinetics. Moreover, under physiological conditions, TMEM16B works as a modulator of the firing behaviors of OSNs.

While TMEM16B exhibits neuronal expression in the OE, TMEM16A seems to be exclusively expressed in the supporting cells, particularly those located in the transition zone within the respiratory epithelium. In supporting cells, TMEM16A may play different roles essential for maintaining ionic and proliferative homeostasis in the OE, possibly via ATP-mediated pathways.

In the vomeronasal sensory epithelium, both TMEM16A and TMEM16B are expressed by the same cellular type, the VSNs responsible for pheromone detection and both proteins co-localize on the apical region and microvilli of VSNs. Although TMEM16A seems to be necessary for the generation of the Ca^{2+}-activated Cl^- currents in VSNs, in physiological conditions, both TMEM16A and TMEM16B play a role in firing behavior in response to natural ligands.

Finally, we summarized the findings about the expression of TMEM16A, but not TMEM16B, in the taste buds of the vallate papillae of the tongue. Despite the detailed biophysical characterization of the Ca^{2+}-activated Cl^- currents in type I taste cells, a clear physiological role of the currents remains elusive. Interestingly, as described for the supporting cells of the OE, TMEM16A may be involved in ATP-mediated signaling in taste bud cells.

The characterization of TMEM16B in the OE has paved the way for studying other TMEM16 channels in various cell types of chemosensory systems. Indeed, while the characterization of the physiological role of TMEM16B in OSNs is extensive, the characterization of the TMEM16A in the supporting cells of the OE, the VSNs and type I taste cells is still in its earlier stages. However, this does not mean that the knowledge of the physiological roles of TMEM16B in OSNs is complete, as for example a deeper understanding of the TMEM16B response kinetics and adaptation is still needed. Furthermore, to better understand the role of TMEM16B in behavior a series of well thought and standardized behavioral tests are needed to unveil its precise physiological roles.

The knowledge acquired on the biophysical and physiological properties of the Ca^{2+}-activated Cl^- currents in the extreme diverse cell types of the chemosensory systems together with different KO animal models could be applied to explore these currents in other epithelial cell types [210]. This approach is particularly timely and significant considering recent advancements in techniques for obtaining human biopsies and cultivating 3D organoids. Such methodologies not only allow to model specific conditions where dysregulated chloride transport is a key factor but also offer a pathway to translational research aimed at addressing respiratory diseases.

Figure Legends

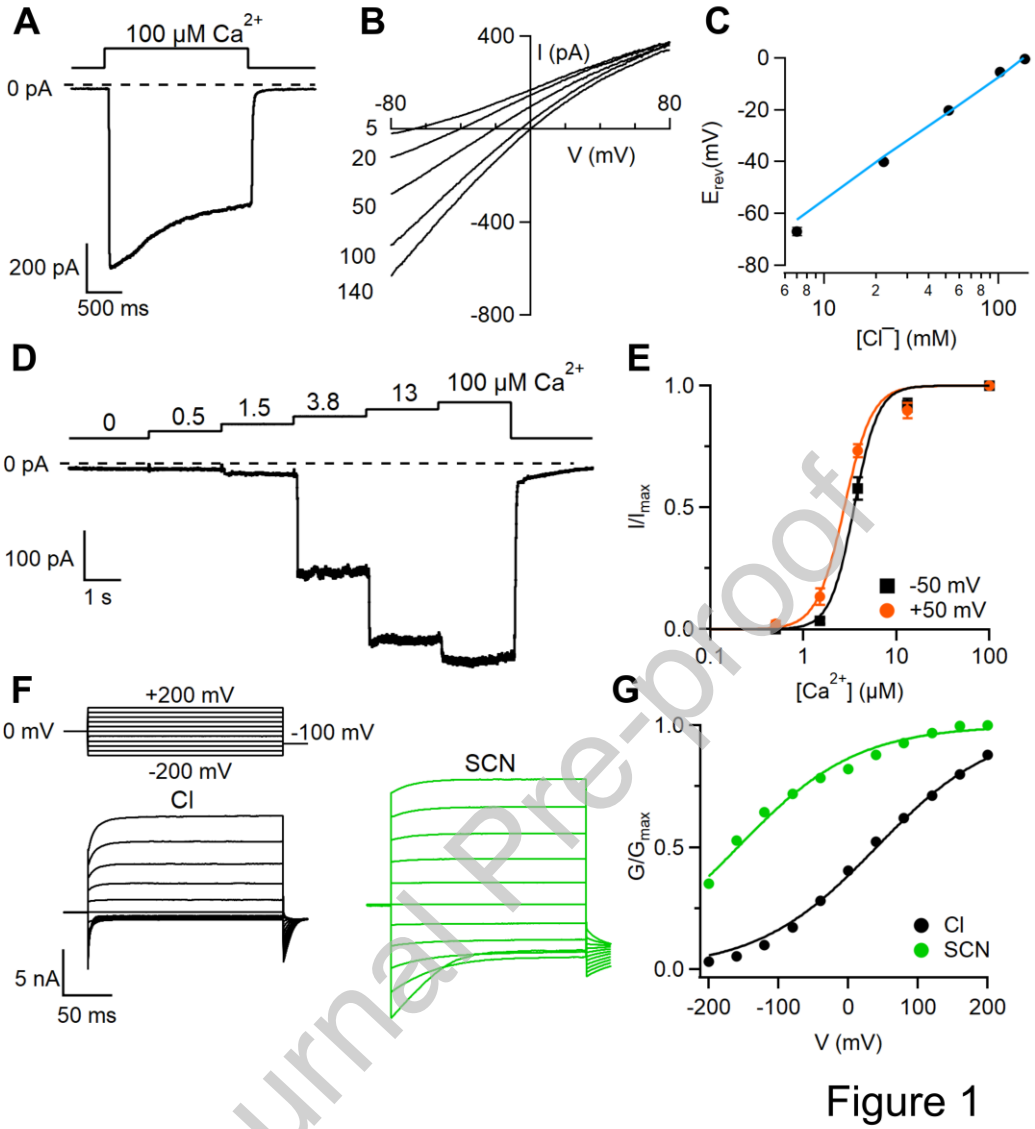

Figure 1

Figure 1. TMEM16B-mediated currents in a heterologous system. (A) An inside-out membrane patch was excised from HEK 293 cells transfected with *Tmem16b* and the cytoplasmic side was exposed to 100 µM Ca^{2+} at the time indicated in the upper trace. The holding potential was −50 mV. **(B)** Current-voltage relations in the inside-out configuration of TMEM16B-mediated current activated by 1 mM Ca^{2+} and a voltage ramp from -100 to +100 mV in the presence of the indicated cytoplasmic concentrations of NaCl. **(C)** Average of reversal potential (E_{rev}) plotted versus $[Cl^-]_i$. The solid lines were calculated according to the Goldman-Hodgkin-Katz equation for a selective Cl^- channel. **(D)** The cytoplasmic side of an inside-out membrane patch was exposed to the indicated free Ca^{2+} concentration at the time indicated in the upper trace. The holding potential was −50 mV. **(E)** Dose–response relations of activation by Ca^{2+} obtained with normalized currents and fitted to the Hill equation. **(F)** TMEM16B-mediated currents in the whole-cell configuration activated by intracellular 1.5 µM free Ca^{2+} recorded in solutions containing NaCl or NaSCN. The voltage protocol is shown on the top of the panel. **(G)** Normalized conductances calculated from tail

currents at -100 mV after prepulses between -200 and +200 mV plotted versus the prepulse voltage. (B-C reprinted from [57]; F-G reprinted from [69]).

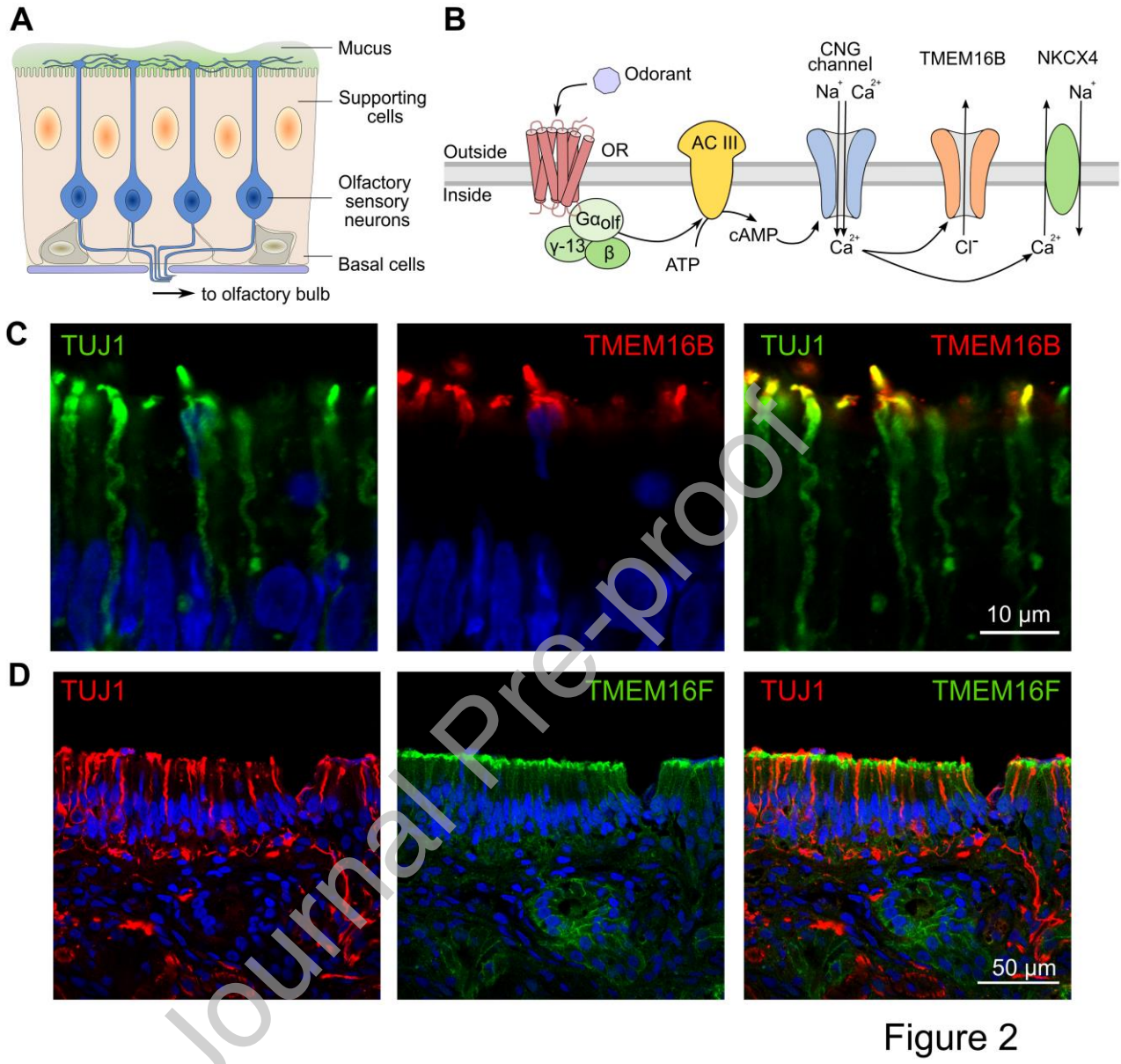

Figure 2

Figure 2. TMEM16B and TMEM16F expression in the human olfactory epithelium. **(A)** Schematic drawing of a coronal section of olfactory epithelium highlighting the different cellular types. **(B)** In the cilia of OSNs, the olfactory transduction cascade begins with the binding of odorant molecules to odorant receptor (OR) inducing the activation of the Gαolf protein leading to the trigger of adenylyl cyclase III (ACIII). ACIII catalyzes the production of cAMP that gates the CNG channel allowing the depolarizing influx of Na^+ and Ca^{2+}. Ca^{2+} induces the opening of TMEM16B channel leading to the efflux of Cl^-, whereas Ca^{2+} is removed by the activity of the Na^+/Ca^{2+} exchanger NKCX4. **(C)** Confocal micrographs of coronal sections of the human olfactory epithelium immunostained for the neuronal marker TUJ1 (green) and TMEM16B (red). TMEM16B is highly expressed in the knob/cilia of OSNs. **(D)** Confocal micrographs of coronal sections of the human olfactory epithelium immunostained for TUJ1 (red) and TMEM16F (green). TMEM16F is highly expressed in the apical region of the olfactory supporting cells and in cells of secretory glands. Cell nuclei were stained by DAPI (blue).(C, reprinted from [110]; D, reprinted from [154]).

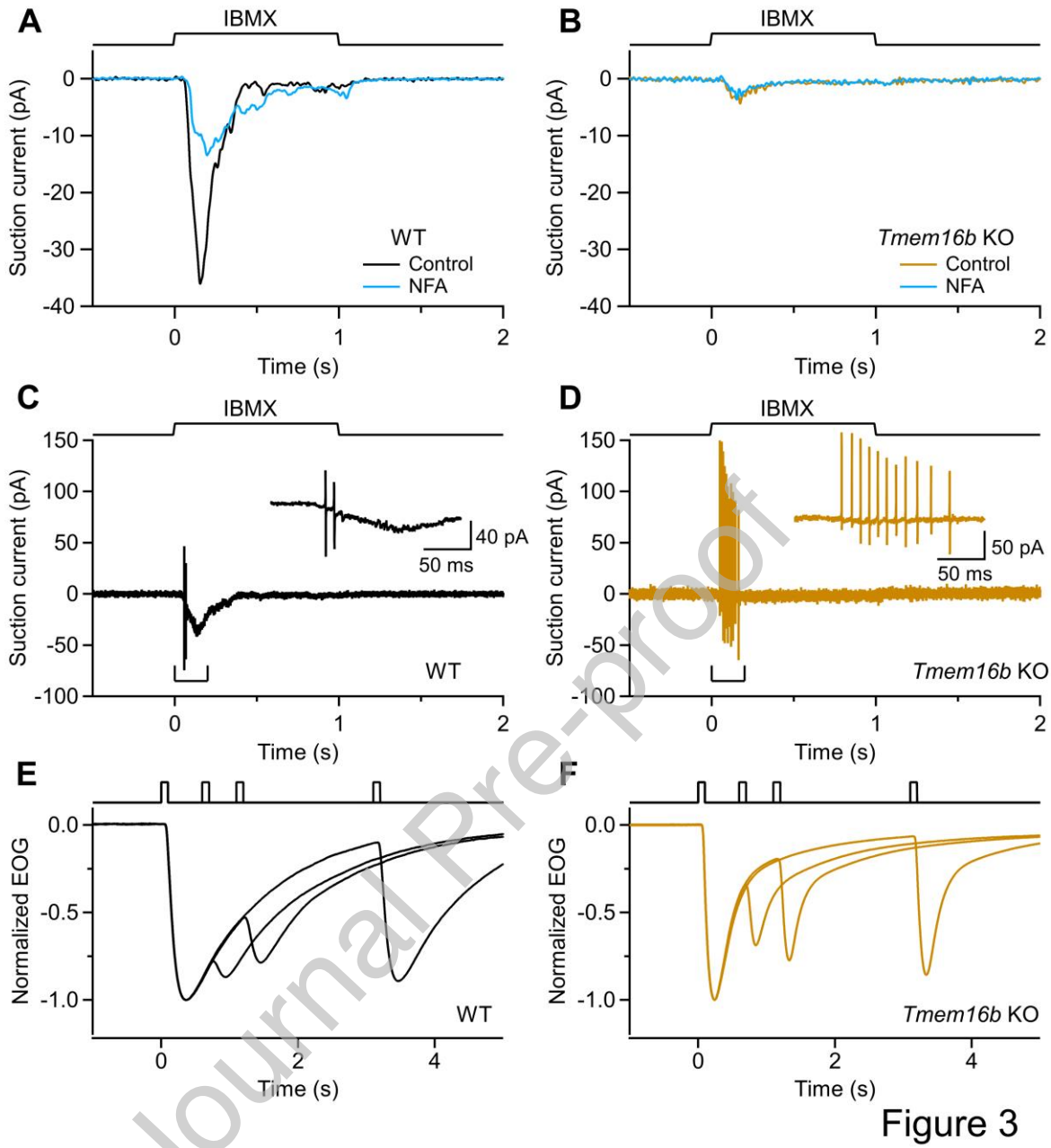

Figure 3

Figure 3. TMEM16B modulates the physiological response of olfactory sensory neurons. Recordings of transduction current **(A-B)** and action potential firing **(C-D)** from isolated OSNs dissociated from the OE of WT and *Tmem16b* KO mice recorded using the suction electrode technique. OSNs were stimulated with the phosphodiesterase inhibitor 3-Isobutyl-1-methylxanthine (IBMX) at 1 mM for 1 s. Recording is **A-B** were performed in control condition and during the application of the Cl^- channel blocker niflumic acid (NFA) at 300 µM. Inserts in C-D show the recordings on an expanded time scale of the indicated regions. **(E-F)** Normalized **e**lectro-olfactogram recordings from the OE of WT and *Tmem16b* KO mice. OEs were stimulated with 100 ms-log pulses of vapor phase of 10^{-2} M solution of the odorant isoamylacetate with different interpulse intervals (0.5, 1, 3 s). (A-D reprinted from [30]; E-F reprinted from [32]).

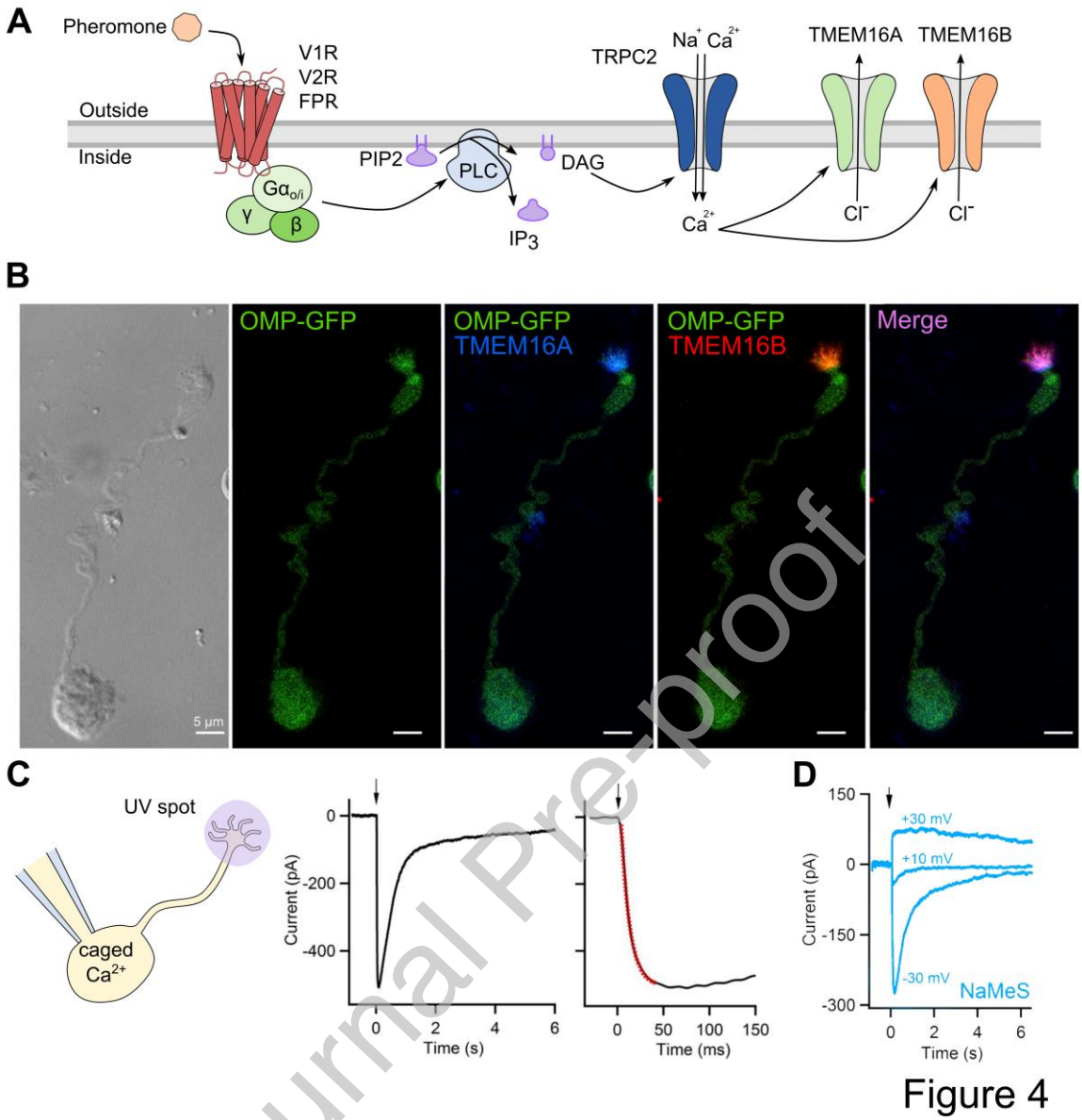

Figure 4

Figure 4. TMEM16A and TMEM16B in vomeronasal sensory neurons. (A) Pheromones and other semiochemicals bind to G-protein coupled receptors expressed by VSNs (V1R, V2R, FPR) leading to the activation of Gαi or Gαo. Gαi/o stimulates the cleavage of phosphatidylinositol bisphosphate (PIP2) to diacylglycerol (DAG) and inositol trisphosphate (IP3) by phospholipase C (PLC). DAG directly gates TRPC2 channels allowing the depolarizing influx of Na^{+} and Ca^{2+}. Ca^{2+} induces the opening of TMEM16A and TMEM16B channels leading to the efflux of Cl^{-}. (**B**) Bright field image of a VSN isolated from an OMP-GFP mouse (left). Confocal micrographs of the same neuron immunostained for TMEM16A (blue) and TMEM16B (red). Cell nuclei were stained by DAPI (blue). **(C)** Schematic drawing of a VSN in the whole-cell configuration filled with caged Ca^{2+}. The circle shows the location of the application of an ultraviolet (UV) flash to photorelease Ca^{2+}(left). At the holding of -50 mV, the application of UV light (arrows) rapidly activated a current. The kinetics of activation waswell fitted by a single exponential function (red dotted line) with a τ value of 9.5 ms. **(D)** Recordings as in **C** at the indicated holding potentials in the presence of an extracellular solution containing sodium methanesulfonate (NaMeS) show that the current induced by photorelease of Ca^{2+} is mainly mediated by Cl^{-}. (B-D reprinted from [178]).

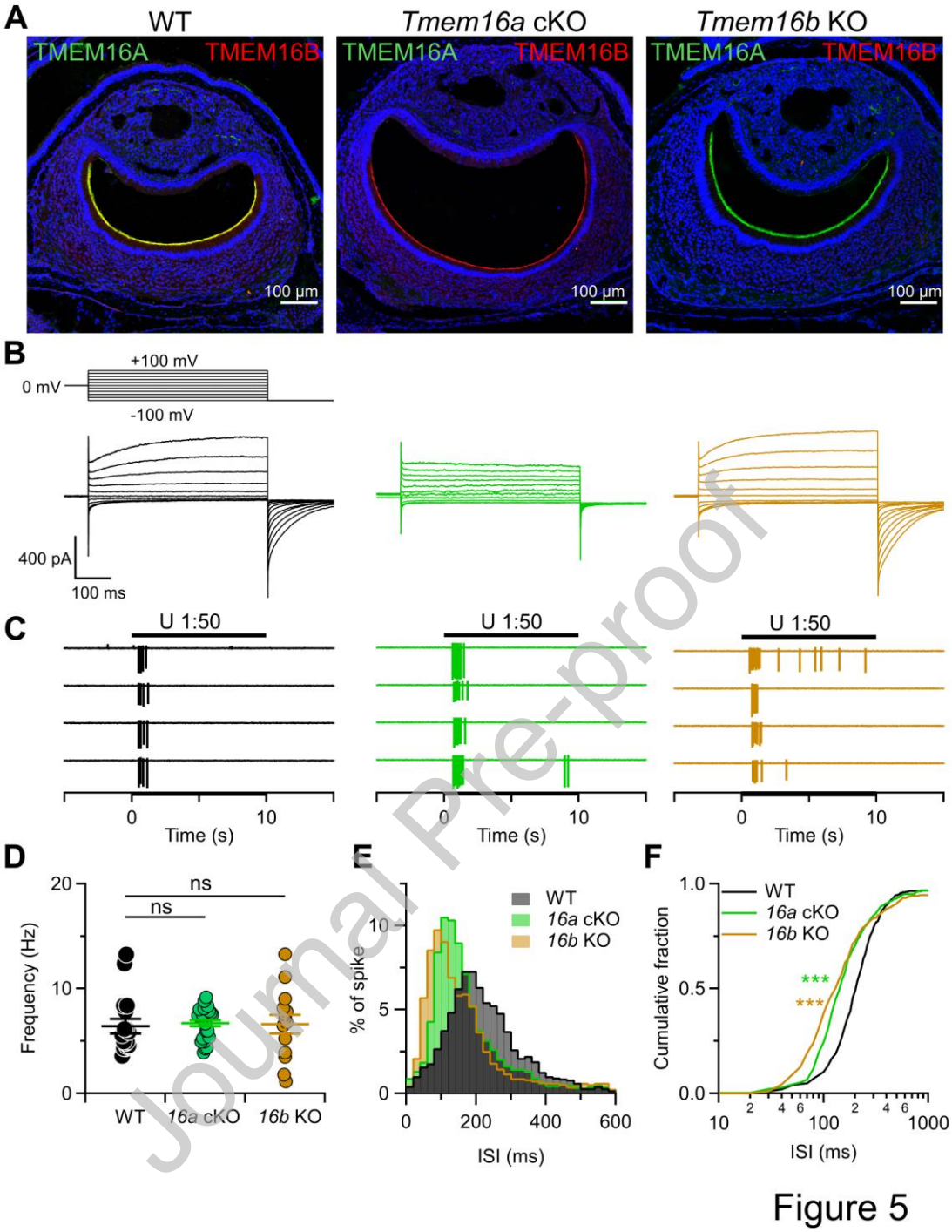

Figure 5

Figure 5. TMEM16A modulates the physiological responses of vomeronasal sensory neurons. **(A)** Confocal micrographs of coronal sections of the vomeronasal organ from WT, *Tmem16a* cKO and *Tmem16b* KO mice immunostained for TMEM16A (green) and TMEM16B (red). Cell nuclei were stained by DAPI (blue). **(B)** Representative whole-cell currents recorded from VSNs from WT (black), *Tmem16a* cKO (green) and *Tmem16b* KO (brown) mice. The intracellular solution contained 1.5 µM free Ca^{2+}. The lack of TMEM16A significantly reduced the Ca^{2+}-dependent current. The voltage protocol is shown at the top left. **(C)** Representative loose-patch recordings from VSNs from WT (black), *Tmem16a* cKO (green) and *Tmem16b* KO (brown) mice stimulated with dilute urine 1:50 (DU). **(D)** Scatter dot plots with average ± SEM of the mean action potential (AP) frequency induced by DU. **(E)** Normalized inter-spike interval (ISI) distributions of firing

activity (20-ms bin width) recorded as in **C**. **(F)** Cumulative fraction of the ISI distributions shown in **E** (***p<0.001, Kolmogorov–Smirnov test; reprinted from [35]).

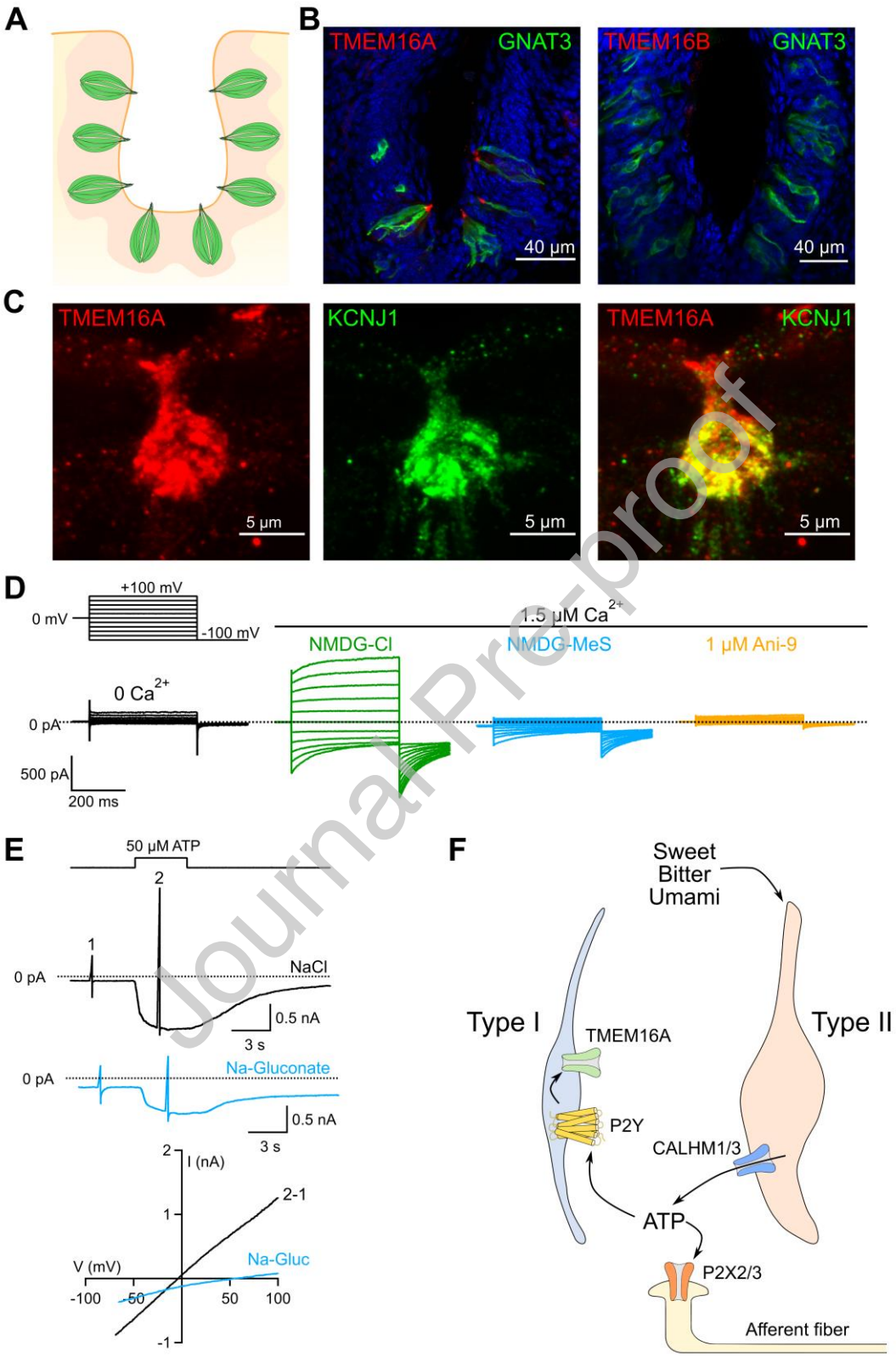

Figure 6

Figure 6. TMEM16A in type I taste cells. (A) Schematic drawing of a coronal section of a vallate papilla showing the distribution of taste buds. **(B)** Confocal micrographs of coronal sections of a vallate papilla immunostained for TMEM16A (red) or TMEM16B (red) and the G-protein alpha subunit gustducin GNAT3, a marker for type II taste cells in taste buds (green). **(C)** Confocal micrographs of coronal sections of a taste bud immunostained for TMEM16A (red) and the inwardly rectifying potassium channel KCNJ1, a marker for type I taste cells (green). Cell nuclei were stained by DAPI (blue). **(D)** Whole-cell recordings from type I taste bud cells. The intracellular solution contained the indicated Ca^{2+} concentration. The voltage protocol is shown at the top left. Recordings with extracellular solution containing N-Methyl-D-glucamine methanesulfonate (NMDG-MeS) show that the Ca^{2+}-activated current is mainly mediated by Cl^{-}. The current was blocked by the TMEM16A blocker Ani-9. **(E)** Whole-cell recordings from type I taste bud cells stimulated with 50 µM ATP at the time indicated in the upper trace. The pipette solution contained NMDG-Cl and nominally 0 Ca^{2+}. The extracellular solutions contained NaCl or NaGluconate, as indicated. Cells were held at -70 mV and voltage ramps from -70 to +100 mV were delivered before (1) and during (2) ATP application. Lower panel: Current-voltage relationships from the cells shown above obtained subtracting the traces (1) from those in the presence of ATP (2). **(G)** Schematic of the proposed mechanism of activation of TMEM16A in type I cells in taste buds. Type II cells are chemosensory cells for sweet, bitter and umami tastants. Their activation induces the release of ATP from CALHM1/3 channels activating P2X2/3 receptors in the afferent fibers. ATP also activates the metabotropic P2Y receptors on type I cells leading to increase in intracellular Ca^{2+} and the activation of TMEM16A. (B-E reprinted from [49]).

References

[1] N. Pedemonte, L.J.V. Galietta, Structure and function of TMEM16 proteins (anoctamins), Physiol. Rev. 94 (2014) 419–459. https://doi.org/10.1152/physrev.00039.2011.

[2] K. Kunzelmann, TMEM16, LRRC8A, bestrophin: chloride channels controlled by Ca(2+) and cell volume, Trends Biochem Sci 40 (2015) 535–543. https://doi.org/10.1016/j.tibs.2015.07.005.

[3] M.E. Falzone, M. Malvezzi, B.-C. Lee, A. Accardi, Known structures and unknown mechanisms of TMEM16 scramblases and channels, J. Gen. Physiol. 150 (2018) 933–947. https://doi.org/10.1085/jgp.201711957.

[4] S.C. Le, P. Liang, A.J. Lowry, H. Yang, Gating and Regulatory Mechanisms of TMEM16 Ion Channels and Scramblases, Front Physiol 12 (2021) 787773. https://doi.org/10.3389/fphys.2021.787773.

[5] B.C. Schroeder, T. Cheng, Y.N. Jan, L.Y. Jan, Expression cloning of TMEM16A as a calcium-activated chloride channel subunit, Cell 134 (2008) 1019–1029. https://doi.org/10.1016/j.cell.2008.09.003.

[6] A. Caputo, E. Caci, L. Ferrera, N. Pedemonte, C. Barsanti, E. Sondo, U. Pfeffer, R. Ravazzolo, O. Zegarra-Moran, L.J.V. Galietta, TMEM16A, a membrane protein associated with calcium-dependent chloride channel activity, Science 322 (2008) 590–594. https://doi.org/10.1126/science.1163518.

[7] Y.D. Yang, H. Cho, J.Y. Koo, M.H. Tak, Y. Cho, W.-S. Shim, S.P. Park, J. Lee, B. Lee, B.-M. Kim, R. Raouf, Y.K. Shin, U. Oh, TMEM16A confers receptor-activated calcium-dependent chloride conductance, Nature 455 (2008) 1210–1215. https://doi.org/10.1038/nature07313.

[8] A.B. Stephan, E.Y. Shum, S. Hirsh, K.D. Cygnar, J. Reisert, H. Zhao, ANO2 is the cilial calcium-activated chloride channel that may mediate olfactory amplification, Proc. Natl. Acad. Sci. U.S.A. 106 (2009) 11776–11781. https://doi.org/10.1073/pnas.0903304106.

[9] S. Pifferi, M. Dibattista, A. Menini, TMEM16B induces chloride currents activated by calcium in mammalian cells, Pflugers Arch. 458 (2009) 1023–1038. https://doi.org/10.1007/s00424-009-0684-9.

[10] J. Suzuki, M. Umeda, P.J. Sims, S. Nagata, Calcium-dependent phospholipid scrambling by TMEM16F, Nature 468 (2010) 834–838. https://doi.org/10.1038/nature09583.

[11] T. Suzuki, J. Suzuki, S. Nagata, Functional swapping between transmembrane proteins TMEM16A and TMEM16F, J. Biol. Chem. 289 (2014) 7438–7447. https://doi.org/10.1074/jbc.M113.542324.

[12] E. Di Zanni, A. Gradogna, J. Scholz-Starke, A. Boccaccio, Gain of function of TMEM16E/ANO5 scrambling activity caused by a mutation associated with gnathodiaphyseal dysplasia, Cell. Mol. Life Sci. 75 (2018) 1657–1670. https://doi.org/10.1007/s00018-017-2704-9.

[13] M.E. Falzone, M. Malvezzi, B.-C. Lee, A. Accardi, Known structures and unknown mechanisms of TMEM16 scramblases and channels, J Gen Physiol 150 (2018) 933–947. https://doi.org/10.1085/jgp.201711957.

[14] S.R. Bushell, A.C.W. Pike, M.E. Falzone, N.J.G. Rorsman, C.M. Ta, R.A. Corey, T.D. Newport, J.C. Christianson, L.F. Scofano, C.A. Shintre, A. Tessitore, A. Chu, Q. Wang, L. Shrestha, S.M.M. Mukhopadhyay, J.D. Love, N.A. Burgess-Brown, R. Sitsapesan, P.J. Stansfeld, J.T. Huiskonen, P. Tammaro, A. Accardi, E.P. Carpenter, The structural basis of lipid scrambling and inactivation in the endoplasmic reticulum scramblase TMEM16K, Nat Commun 10 (2019) 3956. https://doi.org/10.1038/s41467-019-11753-1.

[15] F. Huang, X. Wang, E.M. Ostertag, T. Nuwal, B. Huang, Y.-N. Jan, A.I. Basbaum, L.Y. Jan, TMEM16C facilitates Na(+)-activated K+ currents in rat sensory neurons and regulates pain processing, Nat. Neurosci. 16 (2013) 1284–1290. https://doi.org/10.1038/nn.3468.

[16] A. Jha, W.Y. Chung, L. Vachel, J. Maleth, S. Lake, G. Zhang, M. Ahuja, S. Muallem, Anoctamin 8 tethers endoplasmic reticulum and plasma membrane for assembly of Ca2+ signaling complexes at the ER/PM compartment, EMBO J 38 (2019) e101452. https://doi.org/10.15252/embj.2018101452.

[17] J. Guo, D. Wang, Y. Dong, X. Gao, H. Tong, W. Liu, L. Zhang, M. Sun, ANO7: Insights into topology, function, and potential applications as a biomarker and immunotherapy target, Tissue Cell 72 (2021) 101546. https://doi.org/10.1016/j.tice.2021.101546.

[18] H. Yang, A. Kim, T. David, D. Palmer, T. Jin, J. Tien, F. Huang, T. Cheng, S.R. Coughlin, Y.N. Jan, L.Y. Jan, TMEM16F forms a Ca2+-activated cation channel required for lipid scrambling in platelets during blood coagulation, Cell 151 (2012) 111–122. https://doi.org/10.1016/j.cell.2012.07.036.

[19] S. Grubb, K.A. Poulsen, C.A. Juul, T. Kyed, T.K. Klausen, E.H. Larsen, E.K. Hoffmann, TMEM16F (Anoctamin 6), an anion channel of delayed Ca(2+) activation, J. Gen. Physiol. 141 (2013) 585–600. https://doi.org/10.1085/jgp.201210861.

[20] H. Kim, H. Kim, J. Lee, B. Lee, H.-R. Kim, J. Jung, M.-O. Lee, U. Oh, Anoctamin 9/TMEM16J is a cation channel activated by cAMP/PKA signal, Cell Calcium 71 (2018) 75–85. https://doi.org/10.1016/j.ceca.2017.12.003.

[21] N. Reichhart, S. Schöberl, S. Keckeis, A.S. Alfaar, C. Roubeix, M. Cordes, S. Crespo-Garcia, A. Haeckel, N. Kociok, R. Föckler, G. Fels, A. Mataruga, R. Rauh, V.M. Milenkovic, K. Zühlke, E. Klussmann, E. Schellenberger, O. Strauß, Anoctamin-4 is a bona fide Ca2+-dependent non-selective cation channel, Sci Rep 9 (2019) 2257. https://doi.org/10.1038/s41598-018-37287-y.

[22] S. Stabilini, A. Menini, S. Pifferi, Anion and Cation Permeability of the Mouse TMEM16F Calcium-Activated Channel, Int J Mol Sci 22 (2021) 8578. https://doi.org/10.3390/ijms22168578.

[23] R. Schreiber, I. Uliyakina, P. Kongsuphol, R. Warth, M. Mirza, J.R. Martins, K. Kunzelmann, Expression and function of epithelial anoctamins, J. Biol. Chem. 285 (2010) 7838–7845. https://doi.org/10.1074/jbc.M109.065367.

[24] C. Sagheddu, A. Boccaccio, M. Dibattista, G. Montani, R. Tirindelli, A. Menini, Calcium concentration jumps reveal dynamic ion selectivity of calcium-activated chloride currents in mouse olfactory sensory neurons and TMEM16b-transfected HEK 293T cells, J. Physiol. (Lond.) 588 (2010) 4189–4204. https://doi.org/10.1113/jphysiol.2010.194407.

[25] G.M. Billig, B. Pál, P. Fidzinski, T.J. Jentsch, Ca2+-activated Cl− currents are dispensable for olfaction, Nat. Neurosci. 14 (2011) 763–769. https://doi.org/10.1038/nn.2821.

[26] K. Dauner, J. Lissmann, S. Jeridi, S. Frings, F. Möhrlen, Expression patterns of anoctamin 1 and anoctamin 2 chloride channels in the mammalian nose, Cell Tissue Res. 347 (2012) 327–341. https://doi.org/10.1007/s00441-012-1324-9.

[27] S. Ponissery Saidu, A.B. Stephan, A.K. Talaga, H. Zhao, J. Reisert, Channel properties of the splicing isoforms of the olfactory calcium-activated chloride channel Anoctamin 2, J. Gen. Physiol. 141 (2013) 691–703. https://doi.org/10.1085/jgp.201210937.

[28] D.K. Maurya, A. Menini, Developmental expression of the calcium-activated chloride channels TMEM16A and TMEM16B in the mouse olfactory epithelium, Dev Neurobiol 74 (2014) 657–675. https://doi.org/10.1002/dneu.22159.

[29] D.K. Maurya, T. Henriques, M. Marini, N. Pedemonte, L.J.V. Galietta, J.R. Rock, B.D. Harfe, A. Menini, Development of the Olfactory Epithelium and Nasal Glands in TMEM16A-/- and TMEM16A+/+ Mice, PLoS ONE 10 (2015) e0129171. https://doi.org/10.1371/journal.pone.0129171.

[30] G. Pietra, M. Dibattista, A. Menini, J. Reisert, A. Boccaccio, The Ca2+-activated Cl- channel TMEM16B regulates action potential firing and axonal targeting in olfactory sensory neurons, J. Gen. Physiol. 148 (2016) 293–311. https://doi.org/10.1085/jgp.201611622.
[31] M. Dibattista, S. Pifferi, A. Boccaccio, A. Menini, J. Reisert, The long tale of the calcium activated Cl- channels in olfactory transduction, Channels (Austin) 11 (2017) 399–414. https://doi.org/10.1080/19336950.2017.1307489.
[32] G. Guarneri, S. Pifferi, M. Dibattista, J. Reisert, A. Menini, Paradoxical electro-olfactogram responses in TMEM16B knock-out mice, Chem Senses 48 (2023) bjad003. https://doi.org/10.1093/chemse/bjad003.
[33] A. Amjad, A. Hernandez-Clavijo, S. Pifferi, D.K. Maurya, A. Boccaccio, J. Franzot, J. Rock, A. Menini, Conditional knockout of TMEM16A/anoctamin1 abolishes the calcium-activated chloride current in mouse vomeronasal sensory neurons, J. Gen. Physiol. 145 (2015) 285–301. https://doi.org/10.1085/jgp.201411348.
[34] J. Münch, G. Billig, C.A. Hübner, T. Leinders-Zufall, F. Zufall, T.J. Jentsch, Ca2+-activated Cl- currents in the murine vomeronasal organ enhance neuronal spiking but are dispensable for male-male aggression, J Biol Chem 293 (2018) 10392–10403. https://doi.org/10.1074/jbc.RA118.003153.
[35] A. Hernandez-Clavijo, N. Sarno, K.Y. Gonzalez-Velandia, R. Degen, D. Fleck, J.R. Rock, M. Spehr, A. Menini, S. Pifferi, TMEM16A and TMEM16B Modulate Pheromone-Evoked Action Potential Firing in Mouse Vomeronasal Sensory Neurons, eNeuro 8 (2021) ENEURO.0179-21.2021. https://doi.org/10.1523/ENEURO.0179-21.2021.
[36] H. Stöhr, J.B. Heisig, P.M. Benz, S. Schöberl, V.M. Milenkovic, O. Strauss, W.M. Aartsen, J. Wijnholds, B.H.F. Weber, H.L. Schulz, TMEM16B, a novel protein with calcium-dependent chloride channel activity, associates with a presynaptic protein complex in photoreceptor terminals, J. Neurosci. 29 (2009) 6809–6818. https://doi.org/10.1523/JNEUROSCI.5546-08.2009.
[37] L. Wang, J. Simms, C.J. Peters, M. Tynan-La Fontaine, K. Li, T.M. Gill, Y.N. Jan, L.Y. Jan, TMEM16B Calcium-Activated Chloride Channels Regulate Action Potential Firing in Lateral Septum and Aggression in Male Mice, J Neurosci 39 (2019) 7102–7117. https://doi.org/10.1523/JNEUROSCI.3137-18.2019.
[38] F. Auer, E. Franco Taveras, U. Klein, C. Kesenheimer, D. Fleischhauer, F. Möhrlen, S. Frings, Anoctamin 2-chloride channels reduce simple spike activity and mediate inhibition at elevated calcium concentration in cerebellar Purkinje cells, PLoS One 16 (2021) e0247801. https://doi.org/10.1371/journal.pone.0247801.
[39] K.-X. Li, M. He, W. Ye, J. Simms, M. Gill, X. Xiang, Y.N. Jan, L.Y. Jan, TMEM16B regulates anxiety-related behavior and GABAergic neuronal signaling in the central lateral amygdala, Elife 8 (2019) e47106. https://doi.org/10.7554/eLife.47106.
[40] R. Wang, Y. Lu, M.Z. Cicha, M.V. Singh, C.J. Benson, C.J. Madden, M.W. Chapleau, F.M. Abboud, TMEM16B determines cholecystokinin sensitivity of intestinal vagal afferents of nodose neurons, JCI Insight 4 (2019) e122058. https://doi.org/10.1172/jci.insight.122058.
[41] Y. Zhang, Z. Zhang, S. Xiao, J. Tien, S. Le, T. Le, L.Y. Jan, H. Yang, Inferior Olivary TMEM16B Mediates Cerebellar Motor Learning, Neuron 95 (2017) 1103-1111.e4. https://doi.org/10.1016/j.neuron.2017.08.010.
[42] L. Zhao, L.I. Li, K.-T. Ma, Y. Wang, J. Li, W.-Y. Shi, H.E. Zhu, Z.-S. Zhang, J.-Q. Si, NSAIDs modulate GABA-activated currents via Ca2+-activated Cl- channels in rat dorsal root ganglion neurons, Exp Ther Med 11 (2016) 1755–1761. https://doi.org/10.3892/etm.2016.3158.

[43] W.C. Huang, S. Xiao, F. Huang, B.D. Harfe, Y.N. Jan, L.Y. Jan, Calcium-activated chloride channels (CaCCs) regulate action potential and synaptic response in hippocampal neurons, Neuron 74 (2012) 179–192. https://doi.org/10.1016/j.neuron.2012.01.033.

[44] H. Yamamura, K. Nishimura, Y. Hagihara, Y. Suzuki, Y. Imaizumi, TMEM16A and TMEM16B channel proteins generate Ca2+-activated Cl- current and regulate melatonin secretion in rat pineal glands, J Biol Chem 293 (2018) 995–1006. https://doi.org/10.1074/jbc.RA117.000326.

[45] S. Keckeis, N. Reichhart, C. Roubeix, O. Strauß, Anoctamin2 (TMEM16B) forms the Ca2+-activated Cl- channel in the retinal pigment epithelium, Exp Eye Res 154 (2017) 139–150. https://doi.org/10.1016/j.exer.2016.12.003.

[46] Y. Jang, U. Oh, Anoctamin 1 in secretory epithelia, Cell Calcium 55 (2014) 355–361. https://doi.org/10.1016/j.ceca.2014.02.006.

[47] A. Mata-Daboin, T.A.C. Garrud, C. Fernandez-Pena, D. Peixoto-Neves, M.D. Leo, A.K. Bernardelli, P. Singh, K.U. Malik, J.H. Jaggar, Vasodilators activate the anion channel TMEM16A in endothelial cells to reduce blood pressure, Sci Signal 16 (2023) eadh9399. https://doi.org/10.1126/scisignal.adh9399.

[48] R. Al-Hosni, R. Kaye, C.S. Choi, P. Tammaro, The TMEM16A channel as a potential therapeutic target in vascular disease, Curr Opin Nephrol Hypertens 33 (2024) 161–169. https://doi.org/10.1097/MNH.0000000000000967.

[49] D.M. Guarascio, K.Y. Gonzalez-Velandia, A. Hernandez-Clavijo, A. Menini, S. Pifferi, Functional expression of TMEM16A in taste bud cells, J Physiol 599 (2021) 3697–3714. https://doi.org/10.1113/JP281645.

[50] Y.A. Rodriguez, J.K. Roebber, G. Dvoryanchikov, V. Makhoul, S.D. Roper, N. Chaudhari, “Tripartite Synapses” in Taste Buds: A Role for Type I Glial-like Taste Cells, J Neurosci 41 (2021) 9860–9871. https://doi.org/10.1523/JNEUROSCI.1444-21.2021.

[51] E. Agostinelli, P. Tammaro, Polymodal Control of TMEM16x Channels and Scramblases, Int J Mol Sci 23 (2022) 1580. https://doi.org/10.3390/ijms23031580.

[52] J.D. Brunner, S. Schenck, R. Dutzler, Structural basis for phospholipid scrambling in the TMEM16 family, Curr. Opin. Struct. Biol. 39 (2016) 61–70. https://doi.org/10.1016/j.sbi.2016.05.020.

[53] S. Dang, S. Feng, J. Tien, C.J. Peters, D. Bulkley, M. Lolicato, J. Zhao, K. Zuberbühler, W. Ye, L. Qi, T. Chen, C.S. Craik, Y.N. Jan, D.L. Minor, Y. Cheng, L.Y. Jan, Cryo-EM structures of the TMEM16A calcium-activated chloride channel, Nature 552 (2017) 426–429. https://doi.org/10.1038/nature25024.

[54] C. Paulino, V. Kalienkova, A.K.M. Lam, Y. Neldner, R. Dutzler, Activation mechanism of the calcium-activated chloride channel TMEM16A revealed by cryo-EM, Nature 552 (2017) 421–425. https://doi.org/10.1038/nature24652.

[55] Z. Ye, N. Galvanetto, L. Puppulin, S. Pifferi, H. Flechsig, M. Arndt, C.A.S. Triviño, M. Di Palma, S. Guo, H. Vogel, A. Menini, C.M. Franz, V. Torre, A. Marchesi, Structural heterogeneity of the ion and lipid channel TMEM16F, Nat Commun 15 (2024) 110. https://doi.org/10.1038/s41467-023-44377-7.

[56] V. Cenedese, G. Betto, F. Celsi, O.L. Cherian, S. Pifferi, A. Menini, The voltage dependence of the TMEM16B/anoctamin2 calcium-activated chloride channel is modified by mutations in the first putative intracellular loop, J. Gen. Physiol. 139 (2012) 285–294. https://doi.org/10.1085/jgp.201110764.

[57] S. Pifferi, Permeation Mechanisms in the TMEM16B Calcium-Activated Chloride Channels, PLoS One 12 (2017) e0169572. https://doi.org/10.1371/journal.pone.0169572.

[58] A. Adomaviciene, K.J. Smith, H. Garnett, P. Tammaro, Putative pore-loops of TMEM16/anoctamin channels affect channel density in cell membranes, J. Physiol. (Lond.) 591 (2013) 3487–3505. https://doi.org/10.1113/jphysiol.2013.251660.
[59] Y.-L. Ni, A.-S. Kuan, T.-Y. Chen, Activation and inhibition of TMEM16A calcium-activated chloride channels, PLoS ONE 9 (2014) e86734. https://doi.org/10.1371/journal.pone.0086734.
[60] G. Jeng, M. Aggarwal, W.-P. Yu, T.-Y. Chen, Independent activation of distinct pores in dimeric TMEM16A channels, J. Gen. Physiol. 148 (2016) 393–404. https://doi.org/10.1085/jgp.201611651.
[61] N.K. Lim, A.K.M. Lam, R. Dutzler, Independent activation of ion conduction pores in the double-barreled calcium-activated chloride channel TMEM16A, J. Gen. Physiol. 148 (2016) 375–392. https://doi.org/10.1085/jgp.201611650.
[62] C.J. Peters, J.M. Gilchrist, J. Tien, N.P. Bethel, L. Qi, T. Chen, L. Wang, Y.N. Jan, M. Grabe, L.Y. Jan, The Sixth Transmembrane Segment Is a Major Gating Component of the TMEM16A Calcium-Activated Chloride Channel, Neuron 97 (2018) 1063-1077.e4. https://doi.org/10.1016/j.neuron.2018.01.048.
[63] J. Tien, C.J. Peters, X.M. Wong, T. Cheng, Y.N. Jan, L.Y. Jan, H. Yang, A comprehensive search for calcium binding sites critical for TMEM16A calcium-activated chloride channel activity, Elife 3 (2014). https://doi.org/10.7554/eLife.02772.
[64] C.J. Peters, H. Yu, J. Tien, Y.N. Jan, M. Li, L.Y. Jan, Four basic residues critical for the ion selectivity and pore blocker sensitivity of TMEM16A calcium-activated chloride channels, Proc. Natl. Acad. Sci. U.S.A. 112 (2015) 3547–3552. https://doi.org/10.1073/pnas.1502291112.
[65] A.K.M. Lam, J. Rheinberger, C. Paulino, R. Dutzler, Gating the pore of the calcium-activated chloride channel TMEM16A, Nat Commun 12 (2021) 785. https://doi.org/10.1038/s41467-020-20787-9.
[66] Q. Xiao, K. Yu, P. Perez-Cornejo, Y. Cui, J. Arreola, H.C. Hartzell, Voltage- and calcium-dependent gating of TMEM16A/Ano1 chloride channels are physically coupled by the first intracellular loop, Proc. Natl. Acad. Sci. U.S.A. 108 (2011) 8891–8896. https://doi.org/10.1073/pnas.1102147108.
[67] C.M. Ta, A. Adomaviciene, N.J.G. Rorsman, H. Garnett, P. Tammaro, Mechanism of allosteric activation of TMEM16A/ANO1 channels by a commonly used chloride channel blocker, Br J Pharmacol 173 (2016) 511–528. https://doi.org/10.1111/bph.13381.
[68] P. Perez-Cornejo, J.A. De Santiago, J. Arreola, Permeant anions control gating of calcium-dependent chloride channels, J. Membr. Biol. 198 (2004) 125–133. https://doi.org/10.1007/s00232-004-0659-x.
[69] G. Betto, O.L. Cherian, S. Pifferi, V. Cenedese, A. Boccaccio, A. Menini, Interactions between permeation and gating in the TMEM16B/anoctamin2 calcium-activated chloride channel, J. Gen. Physiol. 143 (2014) 703–718. https://doi.org/10.1085/jgp.201411182.
[70] J.J. De Jesús-Pérez, A.E. López-Romero, O. Posadas, G. Segura-Covarrubias, I. Aréchiga-Figueroa, B. Gutiérrez-Medina, P. Pérez-Cornejo, J. Arreola, Gating and anion selectivity are reciprocally regulated in TMEM16A (ANO1), J Gen Physiol 154 (2022) e202113027. https://doi.org/10.1085/jgp.202113027.
[71] O.L. Cherian, A. Menini, A. Boccaccio, Multiple effects of anthracene-9-carboxylic acid on the TMEM16B/anoctamin2 calcium-activated chloride channel, Biochim Biophys Acta 1848 (2015) 1005–1013. https://doi.org/10.1016/j.bbamem.2015.01.009.

[72] R.L. Dinsdale, T. Pipatpolkai, E. Agostinelli, A.J. Russell, P.J. Stansfeld, P. Tammaro, An outer-pore gate modulates the pharmacology of the TMEM16A channel, Proc Natl Acad Sci U S A 118 (2021) e2023572118. https://doi.org/10.1073/pnas.2023572118.

[73] R. De La Fuente, W. Namkung, A. Mills, A.S. Verkman, Small-molecule screen identifies inhibitors of a human intestinal calcium-activated chloride channel, Mol Pharmacol 73 (2008) 758–768. https://doi.org/10.1124/mol.107.043208.

[74] W. Namkung, P.-W. Phuan, A.S. Verkman, TMEM16A inhibitors reveal TMEM16A as a minor component of calcium-activated chloride channel conductance in airway and intestinal epithelial cells, J Biol Chem 286 (2011) 2365–2374. https://doi.org/10.1074/jbc.M110.175109.

[75] S.-J. Oh, S.J. Hwang, J. Jung, K. Yu, J. Kim, J.Y. Choi, H.C. Hartzell, E.J. Roh, C.J. Lee, MONNA, a potent and selective blocker for transmembrane protein with unknown function 16/anoctamin-1, Mol Pharmacol 84 (2013) 726–735. https://doi.org/10.1124/mol.113.087502.

[76] Y. Seo, H.K. Lee, J. Park, D.-K. Jeon, S. Jo, M. Jo, W. Namkung, Ani9, A Novel Potent Small-Molecule ANO1 Inhibitor with Negligible Effect on ANO2, PLoS ONE 11 (2016) e0155771. https://doi.org/10.1371/journal.pone.0155771.

[77] F. Huang, H. Zhang, M. Wu, H. Yang, M. Kudo, C.J. Peters, P.G. Woodruff, O.D. Solberg, M.L. Donne, X. Huang, D. Sheppard, J.V. Fahy, P.J. Wolters, B.L.M. Hogan, W.E. Finkbeiner, M. Li, Y.-N. Jan, L.Y. Jan, J.R. Rock, Calcium-activated chloride channel TMEM16A modulates mucin secretion and airway smooth muscle contraction, Proc Natl Acad Sci U S A 109 (2012) 16354–16359. https://doi.org/10.1073/pnas.1214596109.

[78] M. Genovese, M. Buccirossi, D. Guidone, R. De Cegli, S. Sarnataro, D. di Bernardo, L.J.V. Galietta, Analysis of inhibitors of the anoctamin-1 chloride channel (transmembrane member 16A, TMEM16A) reveals indirect mechanisms involving alterations in calcium signalling, Br J Pharmacol 180 (2023) 775–785. https://doi.org/10.1111/bph.15995.

[79] C. Zelano, N. Sobel, Humans as an animal model for systems-level organization of olfaction, Neuron 48 (2005) 431–454. https://doi.org/10.1016/j.neuron.2005.10.009.

[80] G.M. Shepherd, Smell images and the flavour system in the human brain, Nature 444 (2006) 316–321. https://doi.org/10.1038/nature05405.

[81] B.P. Menco, Qualitative and quantitative freeze-fracture studies on olfactory and nasal respiratory epithelial surfaces of frog, ox, rat, and dog. II. Cell apices, cilia, and microvilli, Cell Tissue Res. 211 (1980) 5–29. https://doi.org/10.1007/BF00233719.

[82] E.E. Morrison, R.M. Costanzo, Morphology of the human olfactory epithelium, J. Comp. Neurol. 297 (1990) 1–13. https://doi.org/10.1002/cne.902970102.

[83] S. Ualiyeva, E. Lemire, C. Wong, A. Perniss, A.A. Boyd, E.C. Avilés, D.G. Minichetti, A. Maxfield, R. Roditi, I. Matsumoto, X. Wang, W. Deng, N.A. Barrett, K.M. Buchheit, T.M. Laidlaw, J.A. Boyce, L.G. Bankova, A.L. Haber, A nasal cell atlas reveals heterogeneity of tuft cells and their role in directing olfactory stem cell proliferation, Sci Immunol 9 (2024) eabq4341. https://doi.org/10.1126/sciimmunol.abq4341.

[84] M. Khan, S.-J. Yoo, M. Clijsters, W. Backaert, A. Vanstapel, K. Speleman, C. Lietaer, S. Choi, T.D. Hether, L. Marcelis, A. Nam, L. Pan, J.W. Reeves, P. Van Bulck, H. Zhou, M. Bourgeois, Y. Debaveye, P. De Munter, J. Gunst, M. Jorissen, K. Lagrou, N. Lorent, A. Neyrinck, M. Peetermans, D.R. Thal, C. Vandenbriele, J. Wauters, P. Mombaerts, L. Van Gerven, Visualizing in deceased COVID-19 patients how SARS-CoV-2 attacks the respiratory and olfactory mucosae but spares the olfactory bulb, Cell 184 (2021) 5932-5949.e15. https://doi.org/10.1016/j.cell.2021.10.027.

[85] J.E. Schwob, W. Jang, E.H. Holbrook, B. Lin, D.B. Herrick, J.N. Peterson, J. Hewitt Coleman, Stem and progenitor cells of the mammalian olfactory epithelium: Taking poietic license, J Comp Neurol 525 (2017) 1034–1054. https://doi.org/10.1002/cne.24105.

[86] M.A. Durante, S. Kurtenbach, Z.B. Sargi, J.W. Harbour, R. Choi, S. Kurtenbach, G.M. Goss, H. Matsunami, B.J. Goldstein, Single-cell analysis of olfactory neurogenesis and differentiation in adult humans, Nat Neurosci 23 (2020) 323–326. https://doi.org/10.1038/s41593-020-0587-9.

[87] F. Zufall, S. Firestein, Divalent cations block the cyclic nucleotide-gated channel of olfactory receptor neurons, J Neurophysiol 69 (1993) 1758–1768. https://doi.org/10.1152/jn.1993.69.5.1758.

[88] S. Frings, R. Seifert, M. Godde, U.B. Kaupp, Profoundly different calcium permeation and blockage determine the specific function of distinct cyclic nucleotide-gated channels, Neuron 15 (1995) 169–179. https://doi.org/10.1016/0896-6273(95)90074-8.

[89] R.Y.K. Pun, S.J. Kleene, Contribution of cyclic-nucleotide-gated channels to the resting conductance of olfactory receptor neurons, Biophys J 84 (2003) 3425–3435. https://doi.org/10.1016/S0006-3495(03)70064-2.

[90] T. Leinders-Zufall, M.N. Rand, G.M. Shepherd, C.A. Greer, F. Zufall, Calcium entry through cyclic nucleotide-gated channels in individual cilia of olfactory receptor cells: spatiotemporal dynamics, J. Neurosci. 17 (1997) 4136–4148.

[91] T. Leinders-Zufall, C.A. Greer, G.M. Shepherd, F. Zufall, Imaging odor-induced calcium transients in single olfactory cilia: specificity of activation and role in transduction, J Neurosci 18 (1998) 5630–5639. https://doi.org/10.1523/JNEUROSCI.18-15-05630.1998.

[92] S.J. Kleene, R.C. Gesteland, Calcium-activated chloride conductance in frog olfactory cilia, J. Neurosci. 11 (1991) 3624–3629.

[93] T. Kurahashi, K.W. Yau, Co-existence of cationic and chloride components in odorant-induced current of vertebrate olfactory receptor cells, Nature 363 (1993) 71–74. https://doi.org/10.1038/363071a0.

[94] G. Lowe, G.H. Gold, Nonlinear amplification by calcium-dependent chloride channels in olfactory receptor cells, Nature 366 (1993) 283–286. https://doi.org/10.1038/366283a0.

[95] A.B. Zhainazarov, B.W. Ache, Odor-induced currents in Xenopus olfactory receptor cells measured with perforated-patch recording, J. Neurophysiol. 74 (1995) 479–483. https://doi.org/10.1152/jn.1995.74.1.479.

[96] K. Sato, N. Suzuki, The contribution of a Ca(2+)-activated Cl(-) conductance to amino-acid-induced inward current responses of ciliated olfactory neurons of the rainbow trout, J Exp Biol 203 (2000) 253–262. https://doi.org/10.1242/jeb.203.2.253.

[97] J. Reisert, P.J. Bauer, K.-W. Yau, S. Frings, The Ca-activated Cl channel and its control in rat olfactory receptor neurons, J. Gen. Physiol. 122 (2003) 349–363. https://doi.org/10.1085/jgp.200308888.

[98] S. Pifferi, V. Cenedese, A. Menini, Anoctamin 2/TMEM16B: a calcium-activated chloride channel in olfactory transduction, Exp. Physiol. 97 (2012) 193–199. https://doi.org/10.1113/expphysiol.2011.058230.

[99] J. Reisert, J. Lai, K.-W. Yau, J. Bradley, Mechanism of the excitatory Cl- response in mouse olfactory receptor neurons, Neuron 45 (2005) 553–561. https://doi.org/10.1016/j.neuron.2005.01.012.

[100] W.T. Nickell, N.K. Kleene, S.J. Kleene, Mechanisms of neuronal chloride accumulation in intact mouse olfactory epithelium, J. Physiol. (Lond.) 583 (2007) 1005–1020. https://doi.org/10.1113/jphysiol.2007.129601.

[101] D. Reuter, K. Zierold, W.H. Schröder, S. Frings, A depolarizing chloride current contributes to chemoelectrical transduction in olfactory sensory neurons in situ, J. Neurosci. 18 (1998) 6623–6630.
[102] H. Kaneko, T. Nakamura, B. Lindemann, Noninvasive measurement of chloride concentration in rat olfactory receptor cells with use of a fluorescent dye, Am. J. Physiol., Cell Physiol. 280 (2001) C1387-1393. https://doi.org/10.1152/ajpcell.2001.280.6.C1387.
[103] H. Kaneko, I. Putzier, S. Frings, U.B. Kaupp, T. Gensch, Chloride accumulation in mammalian olfactory sensory neurons, J. Neurosci. 24 (2004) 7931–7938. https://doi.org/10.1523/JNEUROSCI.2115-04.2004.
[104] J. Reisert, J. Reingruber, Ca2+-activated Cl- current ensures robust and reliable signal amplification in vertebrate olfactory receptor neurons, Proc. Natl. Acad. Sci. U.S.A. 116 (2019) 1053–1058. https://doi.org/10.1073/pnas.1816371116.
[105] F. Genovese, J. Reisert, V.J. Kefalov, Sensory Transduction in Photoreceptors and Olfactory Sensory Neurons: Common Features and Distinct Characteristics, Front Cell Neurosci 15 (2021) 761416. https://doi.org/10.3389/fncel.2021.761416.
[106] K.D. Cygnar, H. Zhao, Phosphodiesterase 1C is dispensable for rapid response termination of olfactory sensory neurons, Nat. Neurosci. 12 (2009) 454–462. https://doi.org/10.1038/nn.2289.
[107] A.B. Stephan, S. Tobochnik, M. Dibattista, C.M. Wall, J. Reisert, H. Zhao, The Na(+)/Ca(2+) exchanger NCKX4 governs termination and adaptation of the mammalian olfactory response, Nat. Neurosci. 15 (2011) 131–137. https://doi.org/10.1038/nn.2943.
[108] D. Fluegge, L.M. Moeller, A. Cichy, M. Gorin, A. Weth, S. Veitinger, S. Cainarca, S. Lohmer, S. Corazza, E.M. Neuhaus, W. Baumgartner, J. Spehr, M. Spehr, Mitochondrial Ca(2+) mobilization is a key element in olfactory signaling, Nat. Neurosci. 15 (2012) 754–762. https://doi.org/10.1038/nn.3074.
[109] F. Neureither, N. Stowasser, S. Frings, F. Möhrlen, Tracking of unfamiliar odors is facilitated by signal amplification through anoctamin 2 chloride channels in mouse olfactory receptor neurons, Physiol Rep 5 (2017). https://doi.org/10.14814/phy2.13373.
[110] A. Hernandez-Clavijo, C.A. Sánchez Triviño, G. Guarneri, C. Ricci, F.A. Mantilla-Esparza, K.Y. Gonzalez-Velandia, P. Boscolo-Rizzo, M. Tofanelli, P. Bonini, M. Dibattista, G. Tirelli, A. Menini, Shedding light on human olfaction: Electrophysiological recordings from sensory neurons in acute slices of olfactory epithelium, iScience 26 (2023) 107186. https://doi.org/10.1016/j.isci.2023.107186.
[111] R. Schneppenheim, G. Castaman, A.B. Federici, W. Kreuz, R. Marschalek, J. Oldenburg, F. Oyen, U. Budde, A common 253-kb deletion involving VWF and TMEM16B in German and Italian patients with severe von Willebrand disease type 3, Journal of Thrombosis and Haemostasis 5 (2007) 722–728. https://doi.org/10.1111/j.1538-7836.2007.02460.x.
[112] V. Cenedese, M. Mezzavilla, A. Morgan, R. Marino, C.P. Ettorre, M. Margaglione, P. Gasparini, A. Menini, Assessment of the olfactory function in Italian patients with type 3 von Willebrand disease caused by a homozygous 253 Kb deletion involving VWF and TMEM16B/ANO2, PLoS One 10 (2015) e0116483. https://doi.org/10.1371/journal.pone.0116483.
[113] A. Boccaccio, A. Menini, Temporal development of cyclic nucleotide-gated and Ca2+ -activated Cl- currents in isolated mouse olfactory sensory neurons, J. Neurophysiol. 98 (2007) 153–160. https://doi.org/10.1152/jn.00270.2007.
[114] S.J. Kleene, High-gain, low-noise amplification in olfactory transduction, Biophys J 73 (1997) 1110–1117. https://doi.org/10.1016/S0006-3495(97)78143-8.

[115] R.-C. Li, C.-C. Lin, X. Ren, J.S. Wu, L.L. Molday, R.S. Molday, K.-W. Yau, Ca2+-activated Cl current predominates in threshold response of mouse olfactory receptor neurons, Proc. Natl. Acad. Sci. U.S.A. 115 (2018) 5570–5575. https://doi.org/10.1073/pnas.1803443115.
[116] T. Shibuya, S. Shibuya, Olfactory epithelium: unitary responses in the tortoise, Science 140 (1963) 495–496. https://doi.org/10.1126/science.140.3566.495.
[117] R.C. Gesteland, C.D. Sigwart, Olfactory receptor units--a mammalian preparation, Brain Res. 133 (1977) 144–149. https://doi.org/10.1016/0006-8993(77)90055-5.
[118] J. Reisert, H.R. Matthews, Response properties of isolated mouse olfactory receptor cells, J. Physiol. (Lond.) 530 (2001) 113–122. https://doi.org/10.1111/j.1469-7793.2001.0113m.x.
[119] J.-P. Rospars, P. Lansky, M. Chaput, P. Duchamp-Viret, Competitive and noncompetitive odorant interactions in the early neural coding of odorant mixtures, J. Neurosci. 28 (2008) 2659–2666. https://doi.org/10.1523/JNEUROSCI.4670-07.2008.
[120] D. Trotier, Intensity coding in olfactory receptor cells, Semin Cell Biol 5 (1994) 47–54. https://doi.org/10.1006/scel.1994.1007.
[121] F. Kawai, T. Kurahashi, A. Kaneko, Nonselective suppression of voltage-gated currents by odorants in the newt olfactory receptor cells, J Gen Physiol 109 (1997) 265–272. https://doi.org/10.1085/jgp.109.2.265.
[122] J.W. Lynch, P.H. Barry, Action potentials initiated by single channels opening in a small neuron (rat olfactory receptor), Biophys J 55 (1989) 755–768. https://doi.org/10.1016/S0006-3495(89)82874-7.
[123] R.Y.K. Pun, S.J. Kleene, An estimate of the resting membrane resistance of frog olfactory receptor neurones, J Physiol 559 (2004) 535–542. https://doi.org/10.1113/jphysiol.2004.067611.
[124] J.D. Zak, J. Grimaud, R.-C. Li, C.-C. Lin, V.N. Murthy, Calcium-activated chloride channels clamp odor-evoked spike activity in olfactory receptor neurons, Sci Rep 8 (2018) 10600. https://doi.org/10.1038/s41598-018-28855-3.
[125] N. Uchida, Z.F. Mainen, Speed and accuracy of olfactory discrimination in the rat, Nat Neurosci 6 (2003) 1224–1229. https://doi.org/10.1038/nn1142.
[126] N.M. Abraham, H. Spors, A. Carleton, T.W. Margrie, T. Kuner, A.T. Schaefer, Maintaining accuracy at the expense of speed: stimulus similarity defines odor discrimination time in mice, Neuron 44 (2004) 865–876. https://doi.org/10.1016/j.neuron.2004.11.017.
[127] D. Rinberg, A. Koulakov, A. Gelperin, Speed-accuracy tradeoff in olfaction, Neuron 51 (2006) 351–358. https://doi.org/10.1016/j.neuron.2006.07.013.
[128] F. Zufall, T. Leinders-Zufall, The cellular and molecular basis of odor adaptation, Chem. Senses 25 (2000) 473–481. https://doi.org/10.1093/chemse/25.4.473.
[129] T. Kurahashi, A. Menini, Mechanism of odorant adaptation in the olfactory receptor cell, Nature 385 (1997) 725–729. https://doi.org/10.1038/385725a0.
[130] J. Reisert, H.R. Matthews, Adaptation of the odour-induced response in frog olfactory receptor cells, J Physiol 519 Pt 3 (1999) 801–813. https://doi.org/10.1111/j.1469-7793.1999.0801n.x.
[131] S. Firestein, F. Zufall, G.M. Shepherd, Single odor-sensitive channels in olfactory receptor neurons are also gated by cyclic nucleotides, J. Neurosci. 11 (1991) 3565–3572.
[132] J. Bradley, W. Bönigk, K.-W. Yau, S. Frings, Calmodulin permanently associates with rat olfactory CNG channels under native conditions, Nat. Neurosci. 7 (2004) 705–710. https://doi.org/10.1038/nn1266.
[133] J. Wei, A.Z. Zhao, G.C. Chan, L.P. Baker, S. Impey, J.A. Beavo, D.R. Storm, Phosphorylation and inhibition of olfactory adenylyl cyclase by CaM kinase II in Neurons: a mechanism for

attenuation of olfactory signals, Neuron 21 (1998) 495–504. https://doi.org/10.1016/s0896-6273(00)80561-9.
[134] T. Leinders-Zufall, M. Ma, F. Zufall, Impaired odor adaptation in olfactory receptor neurons after inhibition of Ca2+/calmodulin kinase II, J Neurosci 19 (1999) RC19. https://doi.org/10.1523/JNEUROSCI.19-14-j0005.1999.
[135] K.D. Cygnar, S.E. Collins, C.H. Ferguson, C. Bodkin-Clarke, H. Zhao, Phosphorylation of adenylyl cyclase III at serine1076 does not attenuate olfactory response in mice, J Neurosci 32 (2012) 14557–14562. https://doi.org/10.1523/JNEUROSCI.0559-12.2012.
[136] T. Kurahashi, T. Shibuya, Ca2(+)-dependent adaptive properties in the solitary olfactory receptor cell of the newt, Brain Res 515 (1990) 261–268. https://doi.org/10.1016/0006-8993(90)90605-b.
[137] J. Reisert, H.R. Matthews, Na+-dependent Ca2+ extrusion governs response recovery in frog olfactory receptor cells, J. Gen. Physiol. 112 (1998) 529–535.
[138] S. Antolin, H.R. Matthews, The effect of external sodium concentration on sodium-calcium exchange in frog olfactory receptor cells, J Physiol 581 (2007) 495–503. https://doi.org/10.1113/jphysiol.2007.131094.
[139] F. Vogalis, C.C. Hegg, M.T. Lucero, Ionic conductances in sustentacular cells of the mouse olfactory epithelium, J. Physiol. (Lond.) 562 (2005) 785–799. https://doi.org/10.1113/jphysiol.2004.079228.
[140] F. Vogalis, C.C. Hegg, M.T. Lucero, Electrical coupling in sustentacular cells of the mouse olfactory epithelium, J. Neurophysiol. 94 (2005) 1001–1012. https://doi.org/10.1152/jn.01299.2004.
[141] J.E. Rash, K.G.V. Davidson, N. Kamasawa, T. Yasumura, M. Kamasawa, C. Zhang, R. Michaels, D. Restrepo, O.P. Ottersen, C.O. Olson, J.I. Nagy, Ultrastructural localization of connexins (Cx36, Cx43, Cx45), glutamate receptors and aquaporin-4 in rodent olfactory mucosa, olfactory nerve and olfactory bulb, J. Neurocytol. 34 (2005) 307–341. https://doi.org/10.1007/s11068-005-8360-2.
[142] Y. Chen, M.L. Getchell, X. Ding, T.V. Getchell, Immunolocalization of two cytochrome P450 isozymes in rat nasal chemosensory tissue, Neuroreport 3 (1992) 749–752.
[143] J. Gu, Q.Y. Zhang, M.B. Genter, T.W. Lipinskas, M. Negishi, D.W. Nebert, X. Ding, Purification and characterization of heterologously expressed mouse CYP2A5 and CYP2G1: role in metabolic activation of acetaminophen and 2,6-dichlorobenzonitrile in mouse olfactory mucosal microsomes, J. Pharmacol. Exp. Ther. 285 (1998) 1287–1295.
[144] G.K. Whitby-Logan, M. Weech, E. Walters, Zonal expression and activity of glutathione S-transferase enzymes in the mouse olfactory mucosa, Brain Res. 995 (2004) 151–157.
[145] G. Ling, J. Gu, M.B. Genter, X. Zhuo, X. Ding, Regulation of cytochrome P450 gene expression in the olfactory mucosa, Chem. Biol. Interact. 147 (2004) 247–258. https://doi.org/10.1016/j.cbi.2004.02.003.
[146] D. Czesnik, D. Schild, J. Kuduz, I. Manzini, Cannabinoid action in the olfactory epithelium, Proc. Natl. Acad. Sci. U.S.A. 104 (2007) 2967–2972. https://doi.org/10.1073/pnas.0609067104.
[147] M.-C. Lacroix, K. Badonnel, N. Meunier, F. Tan, C. Schlegel-Le Poupon, D. Durieux, R. Monnerie, C. Baly, P. Congar, R. Salesse, M. Caillol, Expression of insulin system in the olfactory epithelium: first approaches to its role and regulation, J. Neuroendocrinol. 20 (2008) 1176–1190. https://doi.org/10.1111/j.1365-2826.2008.01777.x.
[148] E. Breunig, I. Manzini, F. Piscitelli, B. Gutermann, V. Di Marzo, D. Schild, D. Czesnik, The endocannabinoid 2-arachidonoyl-glycerol controls odor sensitivity in larvae of Xenopus laevis, J. Neurosci. 30 (2010) 8965–8973. https://doi.org/10.1523/JNEUROSCI.4030-09.2010.

[149] S. Hayoz, C. Jia, C. Hegg, Mechanisms of constitutive and ATP-evoked ATP release in neonatal mouse olfactory epithelium, BMC Neurosci 13 (2012) 53. https://doi.org/10.1186/1471-2202-13-53.
[150] T. Henriques, E. Agostinelli, A. Hernandez-Clavijo, D.K. Maurya, J.R. Rock, B.D. Harfe, A. Menini, S. Pifferi, TMEM16A calcium-activated chloride currents in supporting cells of the mouse olfactory epithelium, J. Gen. Physiol. 151 (2019) 954–966. https://doi.org/10.1085/jgp.201812310.
[151] C.C. Hegg, D. Greenwood, W. Huang, P. Han, M.T. Lucero, Activation of purinergic receptor subtypes modulates odor sensitivity, J. Neurosci. 23 (2003) 8291–8301.
[152] C.C. Hegg, M. Irwin, M.T. Lucero, Calcium store-mediated signaling in sustentacular cells of the mouse olfactory epithelium, Glia 57 (2009) 634–644. https://doi.org/10.1002/glia.20792.
[153] S. Gayle, G. Burnstock, Immunolocalisation of P2X and P2Y nucleotide receptors in the rat nasal mucosa, Cell Tissue Res. 319 (2005) 27–36. https://doi.org/10.1007/s00441-004-0979-2.
[154] A. Hernandez-Clavijo, K.Y. Gonzalez-Velandia, U. Rangaswamy, G. Guarneri, P. Boscolo-Rizzo, M. Tofanelli, N. Gardenal, R. Sanges, M. Dibattista, G. Tirelli, A. Menini, Supporting Cells of the Human Olfactory Epithelium Co-Express the Lipid Scramblase TMEM16F and ACE2 and May Cause Smell Loss by SARS-CoV-2 Spike-Induced Syncytia, Cell Physiol Biochem 56 (2022) 254–269. https://doi.org/10.33594/000000531.
[155] D.H. Brann, T. Tsukahara, C. Weinreb, M. Lipovsek, K. Van den Berge, B. Gong, R. Chance, I.C. Macaulay, H.-J. Chou, R.B. Fletcher, D. Das, K. Street, H.R. de Bezieux, Y.-G. Choi, D. Risso, S. Dudoit, E. Purdom, J. Mill, R.A. Hachem, H. Matsunami, D.W. Logan, B.J. Goldstein, M.S. Grubb, J. Ngai, S.R. Datta, Non-neuronal expression of SARS-CoV-2 entry genes in the olfactory system suggests mechanisms underlying COVID-19-associated anosmia, Sci Adv 6 (2020) eabc5801. https://doi.org/10.1126/sciadv.abc5801.
[156] L. Fodoulian, J. Tuberosa, D. Rossier, M. Boillat, C. Kan, V. Pauli, K. Egervari, J.A. Lobrinus, B.N. Landis, A. Carleton, I. Rodriguez, SARS-CoV-2 Receptors and Entry Genes Are Expressed in the Human Olfactory Neuroepithelium and Brain, iScience 23 (2020) 101839. https://doi.org/10.1016/j.isci.2020.101839.
[157] J. Lan, J. Ge, J. Yu, S. Shan, H. Zhou, S. Fan, Q. Zhang, X. Shi, Q. Wang, L. Zhang, X. Wang, Structure of the SARS-CoV-2 spike receptor-binding domain bound to the ACE2 receptor, Nature 581 (2020) 215–220. https://doi.org/10.1038/s41586-020-2180-5.
[158] D.W. Sanders, C.C. Jumper, P.J. Ackerman, D. Bracha, A. Donlic, H. Kim, D. Kenney, I. Castello-Serrano, S. Suzuki, T. Tamura, A.H. Tavares, M. Saeed, A.S. Holehouse, A. Ploss, I. Levental, F. Douam, R.F. Padera, B.D. Levy, C.P. Brangwynne, SARS-CoV-2 requires cholesterol for viral entry and pathological syncytia formation, Elife 10 (2021) e65962. https://doi.org/10.7554/eLife.65962.
[159] L. Braga, H. Ali, I. Secco, E. Chiavacci, G. Neves, D. Goldhill, R. Penn, J.M. Jimenez-Guardeño, A.M. Ortega-Prieto, R. Bussani, A. Cannatà, G. Rizzari, C. Collesi, E. Schneider, D. Arosio, A.M. Shah, W.S. Barclay, M.H. Malim, J. Burrone, M. Giacca, Drugs that inhibit TMEM16 proteins block SARS-CoV-2 spike-induced syncytia, Nature 594 (2021) 88–93. https://doi.org/10.1038/s41586-021-03491-6.
[160] M.M. Rajah, A. Bernier, J. Buchrieser, O. Schwartz, The Mechanism and Consequences of SARS-CoV-2 Spike-Mediated Fusion and Syncytia Formation, J Mol Biol 434 (2022) 167280. https://doi.org/10.1016/j.jmb.2021.167280.
[161] M. Zazhytska, A. Kodra, D.A. Hoagland, J. Frere, J.F. Fullard, H. Shayya, N.G. McArthur, R. Moeller, S. Uhl, A.D. Omer, M.E. Gottesman, S. Firestein, Q. Gong, P.D. Canoll, J.E. Goldman,

P. Roussos, B.R. tenOever, null Jonathan B Overdevest, S. Lomvardas, Non-cell-autonomous disruption of nuclear architecture as a potential cause of COVID-19-induced anosmia, Cell 185 (2022) 1052-1064.e12. https://doi.org/10.1016/j.cell.2022.01.024.

[162] R. Tirindelli, M. Dibattista, S. Pifferi, A. Menini, From pheromones to behavior, Physiol. Rev. 89 (2009) 921–956. https://doi.org/10.1152/physrev.00037.2008.

[163] S.D. Liberles, Mammalian pheromones, Annu Rev Physiol 76 (2014) 151–175. https://doi.org/10.1146/annurev-physiol-021113-170334.

[164] J. Mohrhardt, M. Nagel, D. Fleck, Y. Ben-Shaul, M. Spehr, Signal Detection and Coding in the Accessory Olfactory System, Chem Senses 43 (2018) 667–695. https://doi.org/10.1093/chemse/bjy061.

[165] R. Tirindelli, Coding of pheromones by vomeronasal receptors, Cell Tissue Res 383 (2021) 367–386. https://doi.org/10.1007/s00441-020-03376-6.

[166] C. Hamacher, R. Degen, M. Franke, V.K. Switacz, D. Fleck, R.R. Katreddi, A. Hernandez-Clavijo, M. Strauch, N. Horio, E. Hachgenei, J. Spehr, S.D. Liberles, D. Merhof, P.E. Forni, G. Zimmer-Bensch, Y. Ben-Shaul, M. Spehr, A revised conceptual framework for mouse vomeronasal pumping and stimulus sampling, Curr Biol (2024) S0960-9822(24)00034–4. https://doi.org/10.1016/j.cub.2024.01.036.

[167] K. Touhara, L.B. Vosshall, Sensing odorants and pheromones with chemosensory receptors, Annu Rev Physiol 71 (2009) 307–332. https://doi.org/10.1146/annurev.physiol.010908.163209.

[168] P. Mombaerts, Genes and ligands for odorant, vomeronasal and taste receptors, Nat. Rev. Neurosci. 5 (2004) 263–278. https://doi.org/10.1038/nrn1365.

[169] P. Chamero, T. Leinders-Zufall, F. Zufall, From genes to social communication: molecular sensing by the vomeronasal organ, Trends Neurosci. 35 (2012) 597–606. https://doi.org/10.1016/j.tins.2012.04.011.

[170] S. Francia, S. Pifferi, A. Menini, R. Tirindelli, Vomeronasal Receptors and Signal Transduction in the Vomeronasal Organ of Mammals, in: C. Mucignat-Caretta (Ed.), Neurobiology of Chemical Communication, CRC Press/Taylor & Francis, Boca Raton (FL), 2014. http://www.ncbi.nlm.nih.gov/books/NBK200993/ (accessed May 10, 2016).

[171] P. Lucas, K. Ukhanov, T. Leinders-Zufall, F. Zufall, A diacylglycerol-gated cation channel in vomeronasal neuron dendrites is impaired in TRPC2 mutant mice: mechanism of pheromone transduction, Neuron 40 (2003) 551–561. https://doi.org/10.1016/s0896-6273(03)00675-5.

[172] T. Leinders-Zufall, U. Storch, K. Bleymehl, M. Mederos Y Schnitzler, J.A. Frank, D.B. Konrad, D. Trauner, T. Gudermann, F. Zufall, PhoDAGs Enable Optical Control of Diacylglycerol-Sensitive Transient Receptor Potential Channels, Cell Chem Biol 25 (2018) 215-223.e3. https://doi.org/10.1016/j.chembiol.2017.11.008.

[173] E.R. Liman, Regulation by voltage and adenine nucleotides of a Ca2+-activated cation channel from hamster vomeronasal sensory neurons, J Physiol 548 (2003) 777–787. https://doi.org/10.1113/jphysiol.2002.037119.

[174] J. Spehr, S. Hagendorf, J. Weiss, M. Spehr, T. Leinders-Zufall, F. Zufall, Ca2+ -calmodulin feedback mediates sensory adaptation and inhibits pheromone-sensitive ion channels in the vomeronasal organ, J Neurosci 29 (2009) 2125–2135. https://doi.org/10.1523/JNEUROSCI.5416-08.2009.

[175] S. Kim, L. Ma, K.L. Jensen, M.M. Kim, C.T. Bond, J.P. Adelman, C.R. Yu, Paradoxical contribution of SK3 and GIRK channels to the activation of mouse vomeronasal organ, Nat Neurosci 15 (2012) 1236–1244. https://doi.org/10.1038/nn.3173.

[176] C. Yang, R.J. Delay, Calcium-activated chloride current amplifies the response to urine in mouse vomeronasal sensory neurons, J Gen Physiol 135 (2010) 3–13. https://doi.org/10.1085/jgp.200910265.
[177] S. Kim, L. Ma, C.R. Yu, Requirement of calcium-activated chloride channels in the activation of mouse vomeronasal neurons, Nat Commun 2 (2011) 365. https://doi.org/10.1038/ncomms1368.
[178] M. Dibattista, A. Amjad, D.K. Maurya, C. Sagheddu, G. Montani, R. Tirindelli, A. Menini, Calcium-activated chloride channels in the apical region of mouse vomeronasal sensory neurons, J. Gen. Physiol. 140 (2012) 3–15. https://doi.org/10.1085/jgp.201210780.
[179] V. Untiet, L.M. Moeller, X. Ibarra-Soria, G. Sánchez-Andrade, M. Stricker, E.M. Neuhaus, D.W. Logan, T. Gensch, M. Spehr, Elevated Cytosolic Cl- Concentrations in Dendritic Knobs of Mouse Vomeronasal Sensory Neurons, Chem Senses 41 (2016) 669–676. https://doi.org/10.1093/chemse/bjw077.
[180] S. Kim, L. Ma, J. Unruh, S. McKinney, C.R. Yu, Intracellular chloride concentration of the mouse vomeronasal neuron, BMC Neurosci 16 (2015) 90. https://doi.org/10.1186/s12868-015-0230-y.
[181] S.D. Roper, N. Chaudhari, Taste buds: cells, signals and synapses, Nat. Rev. Neurosci. 18 (2017) 485–497. https://doi.org/10.1038/nrn.2017.68.
[182] S.D. Roper, Encoding Taste: From Receptors to Perception, Handb Exp Pharmacol 275 (2022) 53–90. https://doi.org/10.1007/164_2021_559.
[183] A. Vandenbeuch, T.R. Clapp, S.C. Kinnamon, Amiloride-sensitive channels in type I fungiform taste cells in mouse, BMC Neurosci 9 (2008) 1. https://doi.org/10.1186/1471-2202-9-1.
[184] K. Nomura, M. Nakanishi, F. Ishidate, K. Iwata, A. Taruno, All-Electrical Ca2+-Independent Signal Transduction Mediates Attractive Sodium Taste in Taste Buds, Neuron 106 (2020) 816-829.e6. https://doi.org/10.1016/j.neuron.2020.03.006.
[185] C. Baumer-Harrison, M.A. Raymond, T.A. Myers, K.M. Sussman, S.T. Rynberg, A.P. Ugartechea, D. Lauterbach, T.G. Mast, J.M. Breza, Optogenetic Stimulation of Type I GAD65+ Cells in Taste Buds Activates Gustatory Neurons and Drives Appetitive Licking Behavior in Sodium-Depleted Mice, J Neurosci 40 (2020) 7795–7810. https://doi.org/10.1523/JNEUROSCI.0597-20.2020.
[186] G.Q. Zhao, Y. Zhang, M.A. Hoon, J. Chandrashekar, I. Erlenbach, N.J.P. Ryba, C.S. Zuker, The receptors for mammalian sweet and umami taste, Cell 115 (2003) 255–266.
[187] C. Hisatsune, K. Yasumatsu, H. Takahashi-Iwanaga, N. Ogawa, Y. Kuroda, R. Yoshida, Y. Ninomiya, K. Mikoshiba, Abnormal taste perception in mice lacking the type 3 inositol 1,4,5-trisphosphate receptor, J. Biol. Chem. 282 (2007) 37225–37231. https://doi.org/10.1074/jbc.M705641200.
[188] D. Dutta Banik, L.E. Martin, M. Freichel, A.-M. Torregrossa, K.F. Medler, TRPM4 and TRPM5 are both required for normal signaling in taste receptor cells, Proc Natl Acad Sci U S A 115 (2018) E772–E781. https://doi.org/10.1073/pnas.1718802115.
[189] A. Taruno, K. Nomura, T. Kusakizako, Z. Ma, O. Nureki, J.K. Foskett, Taste transduction and channel synapses in taste buds, Pflugers Arch 473 (2021) 3–13. https://doi.org/10.1007/s00424-020-02464-4.
[190] T.E. Finger, V. Danilova, J. Barrows, D.L. Bartel, A.J. Vigers, L. Stone, G. Hellekant, S.C. Kinnamon, ATP signaling is crucial for communication from taste buds to gustatory nerves, Science 310 (2005) 1495–1499. https://doi.org/10.1126/science.1118435.
[191] W. Ye, R.B. Chang, J.D. Bushman, Y.-H. Tu, E.M. Mulhall, C.E. Wilson, A.J. Cooper, W.S. Chick, D.C. Hill-Eubanks, M.T. Nelson, S.C. Kinnamon, E.R. Liman, The K+ channel KIR2.1 functions

in tandem with proton influx to mediate sour taste transduction, Proc Natl Acad Sci U S A 113 (2016) E229-238. https://doi.org/10.1073/pnas.1514282112.
[192] Y.-H. Tu, A.J. Cooper, B. Teng, R.B. Chang, D.J. Artiga, H.N. Turner, E.M. Mulhall, W. Ye, A.D. Smith, E.R. Liman, An evolutionarily conserved gene family encodes proton-selective ion channels, Science 359 (2018) 1047–1050. https://doi.org/10.1126/science.aao3264.
[193] B. Teng, C.E. Wilson, Y.-H. Tu, N.R. Joshi, S.C. Kinnamon, E.R. Liman, Cellular and Neural Responses to Sour Stimuli Require the Proton Channel Otop1, Curr Biol 29 (2019) 3647-3656.e5. https://doi.org/10.1016/j.cub.2019.08.077.
[194] D.W. McBride, S.D. Roper, Ca(2+)-dependent chloride conductance in Necturus taste cells, J Membr Biol 124 (1991) 85–93. https://doi.org/10.1007/BF01871367.
[195] R. Taylor, S. Roper, Ca(2+)-dependent Cl- conductance in taste cells from Necturus, J Neurophysiol 72 (1994) 475–478. https://doi.org/10.1152/jn.1994.72.1.475.
[196] S.L. Wladkowski, W. Lin, M. McPheeters, S.C. Kinnamon, S. Mierson, A basolateral chloride conductance in rat lingual epithelium, J Membr Biol 164 (1998) 91–101. https://doi.org/10.1007/s002329900396.
[197] M.S. Herness, X.D. Sun, Characterization of chloride currents and their noradrenergic modulation in rat taste receptor cells, J Neurophysiol 82 (1999) 260–271. https://doi.org/10.1152/jn.1999.82.1.260.
[198] Y.V. Kim, Y.V. Bobkov, S.S. Kolesnikov, Adenosine triphosphate mobilizes cytosolic calcium and modulates ionic currents in mouse taste receptor cells, Neurosci Lett 290 (2000) 165–168. https://doi.org/10.1016/s0304-3940(00)01342-2.
[199] G. Dvoryanchikov, M.S. Sinclair, I. Perea-Martinez, T. Wang, N. Chaudhari, Inward rectifier channel, ROMK, is localized to the apical tips of glial-like cells in mouse taste buds, J Comp Neurol 517 (2009) 1–14. https://doi.org/10.1002/cne.22152.
[200] A.P. Cherkashin, A.S. Kolesnikova, M.V. Tarasov, R.A. Romanov, O.A. Rogachevskaja, M.F. Bystrova, S.S. Kolesnikov, Expression of calcium-activated chloride channels Ano1 and Ano2 in mouse taste cells, Pflugers Arch. 468 (2016) 305–319. https://doi.org/10.1007/s00424-015-1751-z.
[201] R. Matsuo, Role of saliva in the maintenance of taste sensitivity, Crit Rev Oral Biol Med 11 (2000) 216–229. https://doi.org/10.1177/10454411000110020501.
[202] J.M. Breza, A.A. Nikonov, R.J. Contreras, Response latency to lingual taste stimulation distinguishes neuron types within the geniculate ganglion, J Neurophysiol 103 (2010) 1771–1784. https://doi.org/10.1152/jn.00785.2009.
[203] R. Martín, R. Bajo-Grañeras, R. Moratalla, G. Perea, A. Araque, Circuit-specific signaling in astrocyte-neuron networks in basal ganglia pathways, Science 349 (2015) 730–734. https://doi.org/10.1126/science.aaa7945.
[204] T. Papouin, J. Dunphy, M. Tolman, J.C. Foley, P.G. Haydon, Astrocytic control of synaptic function, Philos Trans R Soc Lond B Biol Sci 372 (2017) 20160154. https://doi.org/10.1098/rstb.2016.0154.
[205] S.D. Roper, Chemical and electrical synaptic interactions among taste bud cells, Curr Opin Physiol 20 (2021) 118–125. https://doi.org/10.1016/j.cophys.2020.12.004.
[206] G. Dvoryanchikov, Y.A. Huang, R. Barro-Soria, N. Chaudhari, S.D. Roper, GABA, its receptors, and GABAergic inhibition in mouse taste buds, J Neurosci 31 (2011) 5782–5791. https://doi.org/10.1523/JNEUROSCI.5559-10.2011.
[207] D.L. Bartel, S.L. Sullivan, E.G. Lavoie, J. Sévigny, T.E. Finger, Nucleoside triphosphate diphosphohydrolase-2 is the ecto-ATPase of type I cells in taste buds, J Comp Neurol 497 (2006) 1–12. https://doi.org/10.1002/cne.20954.

[208] P. Kofuji, E.A. Newman, Potassium buffering in the central nervous system, Neuroscience 129 (2004) 1043–1054. https://doi.org/10.1016/j.neuroscience.2004.06.008.
[209] M.E. Beckner, A roadmap for potassium buffering/dispersion via the glial network of the CNS, Neurochem Int 136 (2020) 104727. https://doi.org/10.1016/j.neuint.2020.104727.
[210] A. Perniss, B. Boonen, S. Tonack, M. Thiel, K. Poharkar, M.W. Alnouri, M. Keshavarz, T. Papadakis, S. Wiegand, U. Pfeil, K. Richter, M. Althaus, J. Oberwinkler, B. Schütz, U. Boehm, S. Offermanns, T. Leinders-Zufall, F. Zufall, W. Kummer, A succinate/SUCNR1-brush cell defense program in the tracheal epithelium, Sci Adv 9 (2023) eadg8842. https://doi.org/10.1126/sciadv.adg8842.

Declaration of Interest Statement

The authors declare that they have no known competing financial interests or personal relationships that could have appeared to influence the work reported in this article.